Diabetes, Metabolic Syndrome and Obesity

Dovepress
Taylor & Francis Group

Open Access Full Text Article

ORIGINAL RESEARCH

# Inhibition of TWEAK/Fn14 Ameliorates Sarcopenic Obesity by Restoring Mitochondrial Biogenesis via the AMPK/SIRT1/PGC-1α Axis

Saiyare Xuekelati[1,*], Zhuoya Maimaitiwusiman[1,*], Yanying Guo[2], Shuke Guo[1], Qihong Xu[1], Jiayu Ke[1], Lei Xu[1], Yining Yang[3,4], Hongmei Wang[1]

[1]Comprehensive Health Internal Medicine Ward II, People's Hospital of Xinjiang Uygur Autonomous Region, Urumqi, Xinjiang, People's Republic of China; [2]Xinjiang Clinical Research Center for Diabetes, Urumqi, Xinjiang, People's Republic of China; [3]Xinjiang Key Laboratory of Cardiovascular Homeostasis and Regeneration Research, Urumqi, Xinjiang, People's Republic of China; [4]Department of Cardiology, People's Hospital of Xinjiang Uyghur Autonomous Region, Urumqi, 830001, People's Republic of China

*These authors contributed equally to this work

Correspondence: Hongmei Wang, Comprehensive Health Internal Medicine Ward II, People's Hospital of Xinjiang Uygur Autonomous Region, NO. 91, Tianchi Road, Urumqi, Xinjiang, People's Republic of China, Email whmdoctor-xj@xjrmyy.com



**Purpose:** Sarcopenic obesity (SO) represents a critical geriatric syndrome where muscle atrophy and obesity synergistically exacerbate metabolic dysfunction. While the TWEAK/Fn14 pathway is a known regulator of muscle wasting, its specific role and therapeutic potential in the pathogenesis of SO remain unclear.

**Methods:** To mimic the lipid-rich microenvironment of SO, we utilized a "PrePA-Diff" in vitro model where C2C12 myoblasts were exposed to palmitic acid prior to differentiation. In vivo, SO was established by feeding aged (18-month-old) male C57BL/6 mice a high-fat diet (HFD) for 12 weeks. Subsequently, intramuscular injection of Adeno-associated virus (AAV)-shRNA was employed to specifically inhibit TWEAK expression in skeletal muscle. Mitochondrial function, inflammatory profiles, and signaling pathways were assessed using qPCR, Western blotting, ELISA, and functional assays.

**Results:** Our results demonstrate that TWEAK inhibition effectively reverses the SO phenotype, characterized by improved grip strength, reduced adiposity, and lowered systemic inflammation and lipid levels. At the cellular level, TWEAK silencing rescued mitochondrial bioenergetics, indicated by enhanced ATP production and suppressed reactive oxygen species (ROS) generation and calcium influx. Molecularly, these protective effects were accompanied by the downregulation of p38 MAPK phosphorylation and the reactivation of the AMPK/SIRT1/PGC-1α signaling axis, a key driver of mitochondrial biogenesis.

**Conclusion:** Our study identifies the TWEAK/Fn14 axis as a pivotal driver of SO pathology. We conclude that inhibiting TWEAK ameliorates sarcopenic obesity by restoring mitochondrial homeostasis via AMPK/SIRT1/PGC-1α signaling, highlighting TWEAK/Fn14 as a novel therapeutic target for age-related musculoskeletal and metabolic decline.

**Keywords:** sarcopenic obesity, skeletal muscle, aging, TWEAK, mitochondrial function

## Introduction

Given the rapid expansion of the elderly population worldwide, age-related health issues have emerged as a critical global concern, with sarcopenia recognized as a widely prevalent condition in older adults.[1] Currently, approximately 50 million people worldwide are affected by sarcopenia; however, this number is projected to rise significantly to 500 million by 2050,[2] highlighting an urgent public health challenge. According to a recent meta-analysis, the prevalence of muscle wasting in the general population aged over 60 ranges from 10% to 40%.[3] Sarcopenia, characterized by the loss of skeletal muscle mass and function, is a multifactorial geriatric syndrome associated with increased vulnerability to adverse outcomes, including falls, frailty, and mortality. Moreover, aging is frequently accompanied by an increase in body fat percentage, predisposing older adults to obesity.[4] The co-existence of excess adiposity and low muscle function is defined as sarcopenic obesity (SO).[5] SO is

https://doi.org/10.2147/DMSO.S596507
Received: 30 January 2026
Accepted: 5 May 2026
Published: 18 May 2026

associated with severe clinical complications, including cardiovascular diseases, metabolic syndrome, and elevated mortality risk. Currently, ~11% of older adults are estimated to suffer from SO globally, a prevalence that increases dramatically after 70 years of age.[6] Although sarcopenia and obesity are distinct conditions, they share common pathophysiological drivers, such as chronic inflammation, oxidative stress, and hormonal senescence. Furthermore, these conditions act synergistically to exacerbate one another, resulting in a "vicious cycle" of metabolic decline. Despite extensive research, the precise molecular pathogenesis of SO remains incompletely understood, and targeted pharmacological therapies are currently lacking. Given the complex inflammatory crosstalk between adipose tissue and skeletal muscle, identifying druggable extracellular targets that can simultaneously alleviate lipotoxicity and restore muscle metabolism is of paramount clinical importance.[7] Emerging evidence suggests that imbalances in skeletal muscle mitochondrial homeostasis, intramuscular lipid infiltration, and inflammation are central to muscle loss.[8] Mitochondrial biogenesis—the process of mitochondrial proliferation and renewal—is crucial for maintaining mitochondrial quality and quantity. During aging, impairments in this process compromise the metabolic homeostasis of skeletal muscle and adipocytes, thereby contributing to the development of SO.[9]

Peroxisome proliferator-activated receptor (PPAR)-γ coactivator 1α (PGC-1α) acts as a central regulator of skeletal muscle fiber composition, mitochondrial content, and oxidative metabolism, maintaining glucose and lipid homeostasis in response to physiological demands.[10–12] PGC-1α orchestrates the transcription of genes related to mitochondrial respiration and biogenesis, thus playing a pivotal role in mtDNA replication and protein synthesis.[13] Studies in transgenic mice have shown that overexpression of PGC-1α in skeletal muscle enhances mitochondrial biogenesis and oxidative capacity, conferring resistance to fatigue and improving aerobic performance.[14,15] Conversely, PGC-1α gene knockout results in the upregulation of muscle atrophy-related genes.[16] In both aged human and animal muscle tissues, PGC-1α expression is typically downregulated, leading to compromised mitochondrial biogenesis. Notably, restoring PGC-1α activity has been suggested to delay the onset and progression of sarcopenia by promoting mitochondrial renewal.[17]

Silent information regulator 1 (SIRT1), a $NAD^+$-dependent deacetylase, functions as a critical upstream modulator of mitochondrial homeostasis in aging skeletal muscle.[18] SIRT1 regulates the transcriptional activity of PGC-1α; specifically, suppression of SIRT1 expression leads to decreased PGC-1α activity, thereby inhibiting the SIRT1/PGC-1α signaling axis and impairing mitochondrial biogenesis.[19] Evidence suggests that SIRT1/PGC-1α-mediated mitochondrial biogenesis can rescue high-fat diet (HFD)-induced mitochondrial dysfunction in skeletal muscle.[20] Furthermore, numerous in vitro and ex vivo experiments have implicated SIRT1 as a key mediator of energy metabolism due to its ability to deacetylate and activate nuclear PGC-1α.[21] Upstream of this complex is adenosine monophosphate-activated protein kinase (AMPK).[22] As a cellular energy sensor, AMPK promotes mitochondrial biogenesis primarily by targeting the SIRT1/PGC-1α axis.[22] Consequently, the AMPK/SIRT1/PGC-1α signaling cascade functions as an integrated energy-sensing network, playing a crucial regulatory role in mitochondrial biosynthesis, metabolic adaptation, and oxidative stress defense.[23] Crucially, this upstream energetic network is highly vulnerable to pro-inflammatory cytokines, such as tumor necrosis factor-α (TNF-α), which are chronically elevated in the SO microenvironment, leading to the profound suppression of PGC-1α-driven mitochondrial renewal.[24]

Tumor necrosis factor-like weak inducer of apoptosis (TWEAK) and its receptor, fibroblast growth factor-inducible 14 (Fn14), constitute a signaling pathway that plays a critical role in regulating denervation-induced muscle atrophy, as well as muscle proliferation, differentiation, and metabolism.[25,26] However, while the catabolic role of TWEAK is well-documented in denervation or cancer cachexia, its specific contribution to the unique, synergistic lipotoxic and age-related inflammatory environment of SO remains a critical knowledge gap. It has been reported that the TWEAK/Fn14 axis functions upstream of the SIRT1/PGC-1α pathway, where TWEAK acts to suppress PGC-1α expression and compromise mitochondrial function.[27] Transcriptomic profiling by Panguluri et al indicated that TWEAK is likely involved in dysregulating myofiber generation, oxidative stress responses, and mitochondrial synthesis.[28] Consistent with this, Fn14 knockout attenuates muscle atrophy and improves muscle function in mice, while TWEAK antagonists significantly block this pathway to protect skeletal muscle structure and function.[29] In the context of metabolic disease, elevated TWEAK concentrations can exacerbate muscle wasting, central obesity, insulin resistance, and metabolic disorders.[30] Compared to TWEAK-knockout mice, wild-type mice exhibit an earlier and more frequent onset of sarcopenic phenotypes. Furthermore, administering high concentrations of TWEAK to knockout mice significantly increases the incidence of muscle atrophy.[31] Building on our previous clinical findings that elevated peripheral blood TWEAK levels correlate with sarcopenia,[32] we further demonstrated that TWEAK/

Fn14 hypomethylation contributes to SO pathogenesis. This epigenetic dysregulation, coupled with increased plasma enrichment of TWEAK and TNF-α, appears to collectively drive SO development.[33] Despite these compelling mechanistic associations, it remains unknown whether targeted genetic blockade of TWEAK in vivo can actively reverse the established SO phenotype, and whether such therapeutic benefits are directly dependent on the reactivation of the AMPK/SIRT1/PGC-1α mitochondrial bioenergetic network. Addressing this question is crucial for translating TWEAK/Fn14 antagonism from a correlative observation into a viable clinical intervention for age-related metabolic decline, especially given that anti-TWEAK neutralizing antibodies have already demonstrated favorable safety profiles in human clinical trials for other chronic inflammatory conditions.[34] Therefore, we hypothesize that targeted inhibition of the TWEAK/Fn14 signaling axis attenuates sarcopenic obesity by reactivating the AMPK/SIRT1/PGC-1α pathway, thereby rescuing mitochondrial biogenesis and reversing muscle-metabolic dysfunction. To test this hypothesis, we employed an SO mouse model induced by feeding aged C57BL/6 mice a high-fat diet, which effectively recapitulates the dual burden of aging and metabolic stress seen in humans. Using this physiologically relevant model alongside well-established in vitro cellular systems, we investigated the therapeutic potential of AAV-mediated muscle-specific TWEAK silencing and elucidated its underlying molecular mechanisms.

# Materials and Methods

## Study Design Overview

To comprehensively investigate the therapeutic effects and underlying mechanisms of TWEAK/Fn14 inhibition on SO, we designed a stepwise study encompassing both in vitro and in vivo models. First, C2C12 myoblasts were utilized to simulate the lipid-rich SO cellular microenvironment to assess morphological and mitochondrial changes. Subsequently, an aged mouse model fed a high-fat diet (HFD) was established to evaluate the macroscopic and tissue-level effects of AAV-mediated TWEAK silencing. Finally, molecular biology techniques were employed to elucidate the specific signaling cascades, particularly the AMPK/SIRT1/PGC-1α axis, responsible for these biological effects.

## Ethics Statement

The study protocols were approved by the Experimental Animal Ethics and Welfare Committee of the People's Hospital of Xinjiang Uygur Autonomous Region (reference number: KY2021031726). All animal care and experimental procedures were performed in accordance with the National Standard of the People's Republic of China (GB/T 42011-2022: Laboratory animals-General code of animal welfare), and the reporting of this study is in accordance with the ARRIVE guidelines.

## Cell Culture, Cell Proliferation and Cell Differentiation

To establish an in vitro model of SO and evaluate the impact of lipid accumulation on myogenesis, C2C12 myoblasts (Procell, Wuhan, China) with a confluence rate of 90% were prepared into a $5\times10^4$ cells/mL single-cell suspension using complete medium and seeded into 96-well plates every 24 h. Cell proliferation was measured 24 h after treatment using the Cell Counting Kit-8 (TransGen Biotech, Beijing, China). Following an 8-day culture period with regular medium replacement, the cells were incubated with 100 μL of culture medium containing 10% CCK-8 solution per well at 37°C for 1 h. The absorbance was measured at 450 nm using a microplate reader (Bio-Rad, CA, United States). When cell confluence reached 70%, the medium was switched to Dulbecco's Modified Eagle Medium (DMEM) containing 2% horse serum for incubation (Solarbio, Beijing, China) and incubated for 5 days to promote cell differentiation into myotube cells. Upon successful induction, C2C12 myotubes were treated with 5 μM dexamethasone (DEX) for 24 h to simulate the in vitro sarcopenia model (DEX group). The simulated in vitro obesity model involved treating the differentiated C2C12 myotubes 0.5 mM palmitic acid (PA) for 24 h (PA group). To establish the in vitro SO model, we utilized a "Pre-treatment with PA before differentiation" (PrePA-Diff) approach, which recapitulates the impact of lipid accumulation on myoblast differentiation potential.[35] To ensure that the observed effects were not due to compromised cell viability, C2C12 myoblasts were treated with various concentrations of PA, and viability was assessed using a CCK-8 assay. A concentration of 100 μM PA was found to be non-cytotoxic and was therefore selected for subsequent experiments. For the PrePA-Diff group, myoblasts were pre-treated with 100 μM PA for 24 h prior to

differentiation. Subsequently, myogenic differentiation was induced by incubation in DMEM supplemented with 2% horse serum for 5 days. The medium was replaced daily, and supernatants were collected and stored at −80°C.

## Myosin Heavy Chain Staining

To visually assess myotube differentiation and morphological integrity under lipid-induced stress, myosin heavy chain (MyHC) staining was performed. Upon reaching approximately 90% myotube fusion, C2C12 cells cultured in 24-well plates were fixed with 4% formaldehyde for 10 min at room temperature, washed three times with phosphate-buffered saline (PBS) containing 0.5% Triton X-100, and blocked with 1% BSA for 40 min. Subsequently, cells were incubated with an anti-MyHC primary antibody (1:200; Santa Cruz, Dallas, TX, USA) overnight at 4°C. After three washes with PBS containing 0.5% Triton X-100, cells were incubated with a Goat Anti-Mouse IgG (H+L) secondary antibody at 37°C for 1 h. Finally, cells were washed three times with PBS. Nuclei were counterstained with DAPI to assess cell density and verify monolayer integrity. Images were acquired using a laser scanning confocal microscope.

## Oil Red O Staining

To visualize and verify the extent of intracellular lipid droplet accumulation in the in vitro models, C2C12 myotubes were washed twice with PBS and then incubated with Oil Red O fixative (Solarbio, China) at 37°C for 20 min. The fixative was then discarded, followed by washing twice with distilled water and differentiating in 60% isopropanol for 20s. Finally, the isopropanol was discarded, and the cells were incubated with Oil Red O staining solution for 10 min, after which the staining solution was removed.

## Generation and Use of Short Hairpin (shRNA)-Expressing Lentivirus

To specifically knock down TWEAK expression in vitro and define its functional role in SO pathogenesis, C2C12 myotubes ($1 \times 10^5$ cells/well) from each group were grown in a 12-well plate overnight. Then, C2C12 myotubes were infected with a lentivirus expressing TWEAK-shRNA-28 (5′-TAACCTACTTTGGACTCTTTC-3′), TWEAK-shRNA-29 (5′-GCTCTCCCAGATTCCTTAAAC-3′), and TWEAK-shRNA-30 (5′-GGGTTCAGAGTAACTGAAGAT-3′) separately, alongside a blank control group (Shanghai Genechem Co., Ltd). After 72 h of infection, the culture medium was discarded, and cells were lysed using 1 mL of TRIzol® reagent (Austin, TX, USA). The lysate was homogenized by repeated pipetting to ensure complete cell lysis and then transferred to a 1.5-mL Eppendorf (EP) tube. Total RNA was extracted, and the expression level of TWEAK was detected and analyzed by quantitative reverse transcription polymerase chain reaction (qRT-PCR) to confirm knockout efficiency.

## Measurement of Cell Morphology and Number of Myotubes

To evaluate the overall cytopathic changes and visually confirm the protective impact of TWEAK knockdown on muscle cell structure, C2C12 cells were divided into six groups: normal cultured C2C12 myoblasts as the blank control group, PA group, DEX group, PrePA-Diff group, PrePA-Diff + TWEAK-NC group, and PrePA-Diff + TWEAK-shRNA group. C2C12 cells ($1 \times 10^5$ cells/well) were seeded into a 24-well cell culture dish and cultured at 37°C for 24 h in a 5% $CO_2$ incubator. The cell morphology and myotube quantity of each group were observed under a microscope.

## Mitochondrial Content and Reactive Oxygen Species (ROS) Detection

Because mitochondrial dysfunction and oxidative stress are central to SO pathology, we evaluated mitochondrial network status and ROS generation. According to the manufacturer's instructions, cells were loaded with 500 μL of 100 nM MitoTracker Red (M7512, Thermo, MA, USA) to measure mitochondrial content and with 500 μL of 5 μM MitoSOX Red (M36008, Thermo, MA, USA) to detect the levels of ROS in the mitochondria. After incubating at 37°C for 30 min, the supernatant was removed, followed by washing the cells twice with PBS. The cells were then fixed with 4% paraformaldehyde for 20 min. After washing with PBS twice, cells were counterstained with DAPI for 5 min, and the cell culture slides were then sealed with 50% glycerol. After centrifugation and washing, the resuspended cells were observed using a laser scanning confocal microscope.

## Animal Experiments

To faithfully recapitulate the dual burden of aging and metabolic stress observed in clinical SO patients, we utilized an aged C57BL/6 mouse model subjected to a high-fat diet. The animal study was performed in accordance with the ARRIVE guidelines. Young (4-month-old, body weight 25–28 g, n=6) and old (15-month-old, body weight 30–40 g, n=32) wild-type male C57BL/6 mice were purchased from the Animal Center of Xinjiang Medical University (Xinjiang, China) and PHENOTEK (Shanghai, China), respectively. All mice were acclimated for 1 week in a specific pathogen-free (SPF) facility under controlled conditions: temperature 22°C ± 2°C, 12-h light/12-h dark cycles, with food and water provided ad libitum). Regular environmental disinfection was maintained using alcohol and UV sterilization. To minimize potential confounders, cage locations were rotated weekly, and animal health was monitored daily. Inclusion and exclusion criteria were established a priori. Animals were included if they appeared healthy after acclimation; exclusion criteria included spontaneous tumors or severe health deterioration unrelated to the experimental intervention. However, no animals were excluded in this study.

The study included the following experimental groups:

Control Group (Young Control, n=6): Young male mice were fed a normal diet (12 kcal% fat, 24 kcal% protein, 64 kcal% carbohydrate) for 3 months (from 4 to 7 months of age). Bilateral gastrocnemius muscles were injected with 25 μL of physiological saline at 4 and 6 months of age.

After acclimation, the old mice (n=32) were randomized using a computer-generated random number sequence into two dietary cohorts:

Sarcopenia Model Group (OM, n=8): Old male mice were fed a normal diet for 3 months (15–18 months of age). Bilateral gastrocnemius muscles were injected with 25 μL of physiological saline at 15 and 17 months of age.

Sarcopenic Obesity Cohort (n=24): The remaining old mice (n=24) were fed a HFD (60 kcal% fat, 20 kcal% protein, and 20 kcal% carbohydrate) for 3 months (15–18 months of age) to induce sarcopenic obesity (SO). Prior to viral intervention, the establishment of the SO phenotype (increased fat mass and decreased relative muscle strength) was confirmed. All 24 mice successfully developed the SO phenotype and were included in the subsequent randomization. These mice were then randomly divided into three subgroups (n=8 per group):

HFD-OM Group (n=8): Injected with 25 μL of physiological saline into bilateral gastrocnemius muscles at 15 and 17 months of age.

HFD-OM + NC Group (n=8): Injected with an empty AAV vector [25 μL, $2.5 \times 10^{11}$ genome copies (gc)] into bilateral gastrocnemius muscles at 15 and 17 months of age to control for vector-mediated immunogenicity.

HFD-OM+TWEAK-AAV Group (n=8): Injected with the TWEAK-adeno-associated virus (TWEAK-AAV) vector (25 μL, $2.5 \times 10^{11}$ gc) into bilateral gastrocnemius muscles at 15 and 17 months of age.

To manipulate TWEAK expression locally and accurately evaluate its therapeutic potential in vivo, we utilized targeted intramuscular viral delivery. Prior to intramuscular injections, mice were anesthetized to minimize suffering. The anesthetic mixture was prepared by combining Zoletil 50 (250 mg) with 2.5 mL of xylazine hydrochloride (100 mg/mL) and 22.5 mL of sterile saline, resulting in a final concentration of 10 mg/mL for each component, and was administered at a dose of 50 mg/kg body weight via intraperitoneal injection. Humane endpoints were strictly defined: animals exhibiting rapid weight loss (>20%) or severe distress were to be euthanized.

Investigators assessing outcomes and performing data analysis were blinded to group allocation. Sample size determination was performed using G*Power software (version 3.1) based on preliminary data for grip strength, with an alpha level of 0.05 and a power of 0.80.

## Measurement of Grip Strength and Body Composition

To evaluate the functional decline and macroscopic physical alterations characteristic of SO, behavioral and compositional assessments were conducted. Briefly, mice were tested to determine their forelimb grip strength using a mouse grip tester (HuaiBei 900 Electronic Technology Co., Ltd, HuaiBei, China) according to the manufacturer's instructions. Mice were placed on the grid and held by their tail such that their forelimbs could grasp the grid. The mice were pulled back by the tail gently until they released the grid. The test was repeated five times to obtain valid readings. The average value

was recorded as the grip strength of the mouse. Body composition was measured by dual-energy X-ray absorptiometry (DXA, BRUKER Minispec LF90II). Mice were anesthetized with 2.5% isoflurane and placed in a prone position on the specimen tray. The skull was excluded from the analysis. Measurements acquired included fat mass (g) and lean mass (g).

## Sample Collection

At the end of the behavioral experiments, blood samples were collected from the retro-orbital sinus under anesthesia and centrifuged at 3000 × g for 10 min to obtain serum. Subsequently, all mice were euthanized by intraperitoneal injection of 2% pentobarbital sodium at a dose of 150 mg/kg body weight.

Both gastrocnemius muscles were rapidly excised immediately after euthanasia. The left gastrocnemius muscle was divided into three portions: one portion was fixed in 4% paraformaldehyde for histological analysis, one was fixed in glutaraldehyde for electron microscopy, and the remaining fresh tissue was processed immediately for flow cytometry. The right gastrocnemius muscle was snap-frozen in liquid nitrogen and stored at −80°C for molecular analysis.

## Enzyme-Linked Immunosorbent Assay (ELISA) and Biochemical Index Analysis

To profile the local and systemic inflammatory microenvironment, as well as lipid metabolism dysregulation, cell supernatants and serum were analyzed. Briefly, the above groups of cells or serum were digested with precooled PBS supplemented with a protease inhibitor (Boster Biological Technology, Wuhan, China) and centrifuged at 5000× g for 10 min at 4°C to obtain the supernatant. Next, 100 μL of diluted samples were maintained in each well of pre-coated ELISA plates at 37°C for 90 min, incubated with 100 μL of biotinylated detection antibody for 1 h, and then treated with HRP conjugate diluent for 30 min. Finally, enzyme activity was measured using TMB at 450 nm. The levels of interleukin 6 (IL-6), interleukin 1β (IL-1β), inducible nitric oxide synthase (iNOS), and tumor necrosis factor-α (TNF-α) in the culture supernatant were measured using commercial mouse ELISA kits (70-EK206/3, 70-EK201B/3, CSB-E08326m, and 70-EK282/4, respectively; Multisciences, Hangzhou, China). In addition, total cholesterol (TC), triglyceride (TG), high density lipoprotein cholesterol (HDL-C), and low-density lipoprotein (LDL-C) in the culture supernatant were quantified using a TC assay kit, a TG assay kit, an HDL-C assay kit, and an LDL-C assay kit, respectively (Nanjing Jiancheng Bioengineering Institute, Nanjing, China). The concentrations of IL-6, IL-1β, and TNF-α were measured using a standard curve and expressed as pg/mL, and iNOS was expressed as IU/mL. The concentrations of TC, TG, HDL-C, and LDL-C were calculated using a standard curve and expressed as mmol/L.

## Determination of Adenosine Triphosphate (ATP) Content and ROS Assay

To quantitatively assess mitochondrial bioenergetics and functional output, an ATP assay kit was used to measure the ATP content in the cells according to the manufacturer's instructions (Nanjing Jiancheng Bioengineering Institute, Nanjing, China). The ATP levels were further standardized by protein content. For tissue sample, the gastrocnemius tissue was used to prepare a 10% homogenate. The supernatant was used to measure the protein concentration, and using the above method, its ATP content was determined. ATP content and protein concentrations were determined using the ATP assay kit (Nanjing Jiancheng Bioengineering Institute, Nanjing, China) and the Easy II Protein Quantitative Kit (BCA, TransGen Biotech), respectively. ATP content was measured with a microplate reader. Each experiment was repeated three times.

Concurrently, to assess oxidative damage within the tissue microenvironment, cellular and tissue ROS levels were measured using a fluorescent dye, 2′,7′dichlorofluorescein diacetate (DCFH-DA, Sigma-Aldrich), which is a non-polar compound that is readily diffusible into cells.[36] Cells were washed twice with PBS, and 10-μM DCFH-DA in PBS was added to the wells. The cells were then incubated at 37°C for 30 min. The gastrocnemius tissues of mice were prepared into a single-cell suspension and stained using the same method as mentioned above. The stained cells were analyzed using a fluorescence microplate reader equipped with a 500/525 nm (for cells) or 488/525 nm (for single-cell suspension of tissue) filter and observed under a fluorescence microscope. For flow cytometry analysis of tissue samples, strict gating strategies were applied based on Forward Scatter (FSC) and Side Scatter (SSC) to identify the main cell population and exclude cell debris. Unstained samples were used as negative controls to determine the baseline fluorescence and

eliminate background autofluorescence. To ensure standardization, consistent instrument settings (voltage and gain) were maintained for all samples within each independent experiment. All in vitro experiments were performed in at least three independent biological replicates.

## Measurement of Levels of Intracellular Calcium

Given that intracellular calcium homeostasis is critical for both muscle contraction and mitochondrial metabolic adaptation, we investigated calcium influx. For animal experiments, fresh gastrocnemius muscle tissue was harvested from each group. The tissue was minced and placed on a 200-mesh nylon net secured over a small beaker. The minced tissue was gently ground on the net using ophthalmic forceps or a scraper while continuously rinsing with PBS until the tissue was completely processed. The resulting cell suspension was collected and centrifuged at 500 × g for 10 minutes. The supernatant was discarded, and the pellet was retained. The pellet was washed 1–2 times with PBS.

To quantify the intracellular calcium levels, cell suspensions of gastrocnemius tissue from all groups were preloaded with the fluorescent calcium indicator Fluo-4 AM (500 μL) for 30 min. Excess Fluo-4 AM dye was washed away with PBS, and the fluorescence intensity of Fluo-4 AM was measured by flow cytometry. Gating was performed using FSC/SSC plots to isolate single cells and exclude debris. Unstained cells were used to set the background gate. Data acquisition was performed using standardized parameters across all samples. Data were normalized to the cell number or mean fluorescence intensity (MFI) of the control group to account for variations.

## RNA Extraction, qRT-PCR, and Western Blotting

Finally, to elucidate the precise molecular mechanisms and evaluate the transcriptional and translational expression levels associated with the TWEAK/Fn14 and AMPK/SIRT1/PGC-1α signaling cascades, mRNA and proteins from tissues and cells were quantified. Total RNA was extracted using TRIzol (Ambion, Austin, TX, USA), and RNA concentration was measured. Each RNA sample was reverse transcribed with 5X All-In-One RT MasterMix (abm, CA) according to the manufacturer's protocol. The qRT-PCR was performed with EvaGreen Express 2 × qPCR MasterMix-Low Rox (abm) and specific mouse primers. The data were analyzed using the $2^{-\Delta\Delta Ct}$ threshold cycle method and normalized to mouse actin. The primers used are listed in Table 1.

For the in vitro study, cells from the six groups were lysed in RIPA extraction buffer (Boster, Wuhan, China) supplemented with protease and phosphatase inhibitors, and total proteins were isolated by centrifugation at 6000 × g for 20 min at 4°C. For the in vivo study, gastrocnemius tissues from all groups were homogenized in 400 μL of the same RIPA lysis buffer and centrifuged at 6000 × g for 20 min at 4°C. Protein concentrations of the supernatants were measured using a BCA protein assay kit. Equal amounts of total protein were separated by SDS-PAGE and subsequently transferred onto PVDF membranes. After blocking with 5% skim milk, the membranes were incubated overnight at 4°C with the following primary antibodies: anti-TWEAK (1:800, Abcam), anti-TWEAKR/FN14 (1:800, Abcam), anti-SIRT1 (1:1000, Abcam), anti-PGC-1α (1:1000, Abcam), anti-p38α/MAPK14 (1:800, Abcam), anti-p-p38 (phospho T180 + Y182) (1:800, Abcam), anti-AMPKα (1:800, Cell Signaling Technology), anti-p-AMPK (1:800, Cell Signaling Technology), and anti-β-actin (1:1000, Sino Biological). Then, the membranes were incubated with the corresponding secondary antibodies at 37°C for 1 h. Finally, protein bands were visualized using a chemiluminescence substrate kit (Thermo, MA, USA) and quantified

**Table 1** List of Polymerase Chain Reaction Primers

| Gene | Forward | Reverse |
|---|---|---|
| TWEAK | 5′-TGAGGGAAAGGCTGTCTACC-3′ | 5′-AGCCTTAAGATGAGCCCAGG-3′ |
| Fn14 | 5′-TCCTCGTGTTGGGATTCGG-3′ | 5′-TAGAAACCAGCGCCAAAACC-3′ |
| Mouse actin | 5′-GGCTGTATTCCCCTCCATCG-3′ | 5′-CCAGTTGGTAACAATGCCATGT-3′ |

**Abbreviations**: TWEAK, tumor necrosis factor-like weak inducer of apoptosis; Fn14, fibroblast growth factor-inducible 14.


https://doi.org/10.2147/DMSO.S596507

using ImageJ software (National Institutes of Health, NIH). The expression of each target protein was normalized to β-actin as an internal control.

## Statistical Analysis

Statistical analyses were performed using SPSS Statistics (version 26.0, IBM Corp., Armonk, NY, USA) and GraphPad Prism (version 10.1.2, GraphPad Software, San Diego, CA, USA). The data were expressed as mean ± standard deviation (SD), where n represents the number of mice per group. Normality was assessed using the one-sample Kolmogorov–Smirnov test, while homogeneity of variances was verified with Levene's test. For datasets satisfying both normality and homoscedasticity assumptions, one-way analysis of variance (ANOVA) was performed followed by Tukey's Honest Significant Difference (HSD) post-hoc test. In cases of heterogeneous variances, Tamhane's T2 test was applied. A $P$-value < 0.05 was considered statistically significant. Data visualization and composite figure assembly were finalized in Adobe Illustrator 2022 (Adobe Inc., San Jose, CA, USA). Additionally, the schematic diagram illustrating the proposed molecular mechanism was created using BioRender.com.

# Results

## Establishment and Validation of the in vitro SO Model

To establish an in vitro model of SO, we induced lipid accumulation and muscle atrophy using palmitic acid (PA) and dexamethasone (DEX) under different conditions. Specifically, the SO model (designated as PrePA-Diff) was created by pretreating myoblasts with PA prior to differentiation,[32] whereas the obesity model (PA group) and sarcopenia model (DEX group) were established by treating mature myotubes.

We first validated the in vitro model phenotypes. Immunofluorescence staining revealed that the expression of MyHC, a critical marker of terminal myogenic differentiation, was significantly reduced in both the DEX and PrePA-Diff groups compared to the control (Figure 1A and B). Crucially, nuclear counterstaining with DAPI confirmed that cell density was preserved across groups, indicating that the observed reduction in MyHC reflected impaired differentiation and muscle atrophy rather than overt cytotoxicity. Concurrently, Oil Red O staining demonstrated extensive lipid droplet accumulation in both the PA and PrePA-Diff groups, confirming the obesity phenotype (Figure 1C). These results verify that the PrePA-Diff group successfully recapitulates the pathological features of SO: concomitant muscle atrophy and lipid accumulation.

Next, we examined TWEAK expression across these groups. TWEAK levels were significantly elevated in the PA, DEX, and PrePA-Diff groups compared to controls. Notably, the PrePA-Diff group exhibited the highest TWEAK expression, surpassing both the single-treatment PA and DEX groups (Figure 1D).

To ensure optimal viral transduction efficiency, we first validated the infection conditions using HitransG A/P co-infection reagent and determined the optimal multiplicity of infection (MOI) to be 100. Under these optimized conditions, TWEAK-shRNA-29 demonstrated the highest knockdown efficiency as verified by qRT-PCR and was therefore selected for subsequent experiments (Figure 1E). Microscopic observations of cell morphology and myotube quantity revealed that both the PrePA-Diff group and PrePA-Diff+NC group had significantly fewer myotubes than the PA and DEX groups. Conversely, the PrePA-Diff +TWEAK-shRNA group had significantly more myotubes than the PrePA-Diff and PrePA-Diff+NC groups (Figure 1F and G). The results showed that silencing TWEAK can increase the number of myotubes in the in vitro SO model.

## The Impact of TWEAK Silencing on Grip Strength, Fat Mass, and Lean Mass in SO Mice

Grip strength was assessed as a functional indicator of muscle strength (measured as tensile force). As expected, aged mice in the OM, HFD-OM, and HFD-OM+NC groups exhibited significantly lower grip strength compared to young mice on a normal diet. However, TWEAK silencing notably reversed this decline, with the HFD-OM+TWEAK-AAV group showing significantly higher grip strength than the HFD-OM+NC group (Figure 2A). Regarding body composition, DXA analysis revealed that fat mass was significantly elevated in the HFD-OM+NC and HFD-OM+TWEAK-AAV groups compared to the OM group. Notably, TWEAK silencing effectively attenuated this lipid accumulation, resulting in significantly lower fat content in the HFD-OM+TWEAK-AAV group compared to the HFD-OM+NC group (Figure 2B). In terms of lean mass, although absolute values were higher in all experimental groups compared to the young control group—likely attributable to

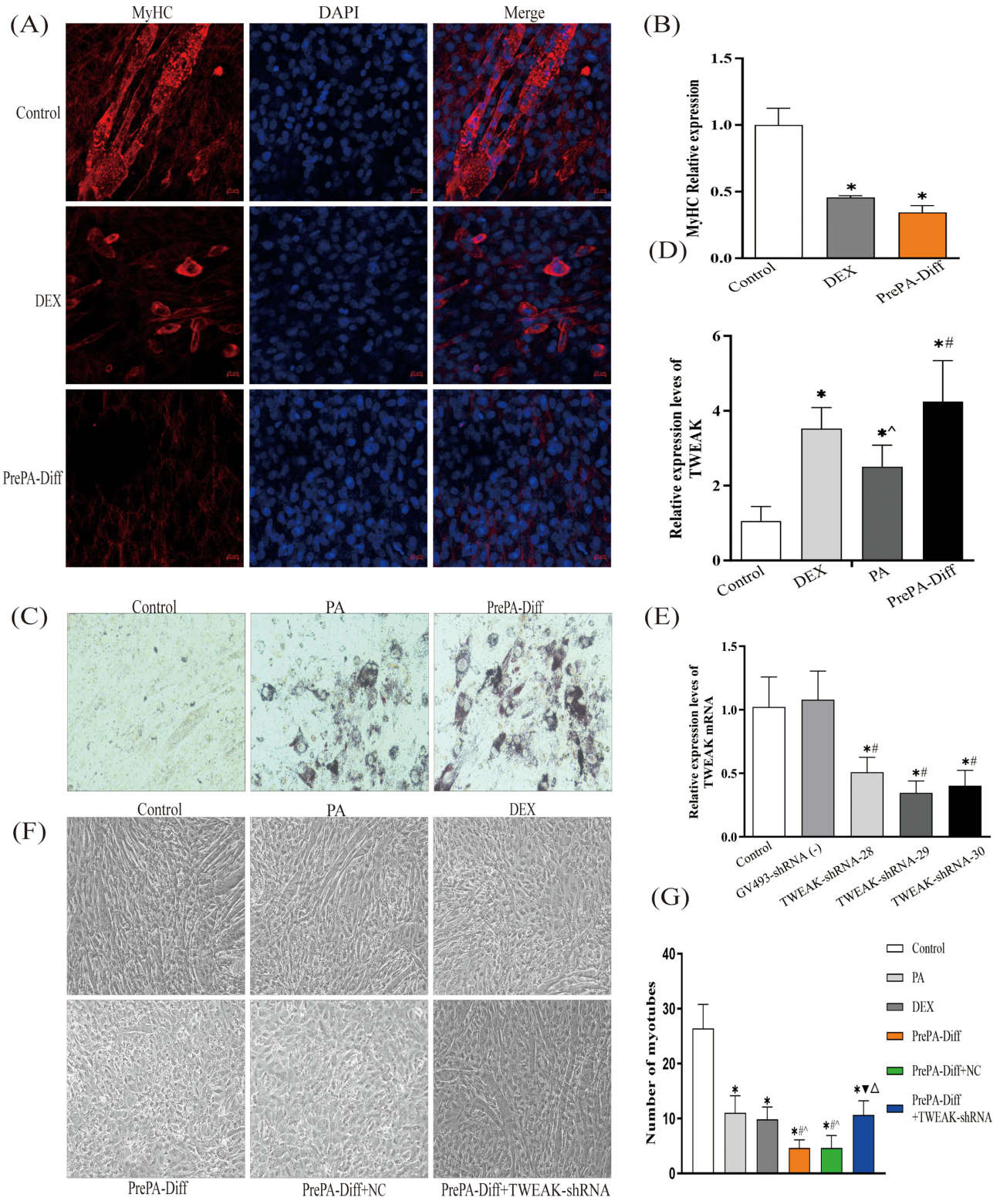


**Figure 1** Establishment of the in vitro sarcopenic obesity (SO) model and evaluation of TWEAK silencing effects. (**A**) Representative immunofluorescence images of myosin heavy chain (MyHC) in C2C12 myotubes (Scale bar = 20 μm). (**B**) Quantitative analysis of MyHC fluorescence intensity indicating muscle atrophy. Data are presented as the mean ± SD (n=3). (**C**) Representative images of lipid accumulation in C2C12 myotubes visualized by Oil Red O staining (Scale bar = 20 μm). (**D**) Relative mRNA expression levels of *TWEAK* in the PA, DEX, and PrePA-Diff groups compared to the control, measured by qRT-PCR. Data are presented as the mean ± SD (n=5). (**E**) Validation of knockdown efficiency for different TWEAK-shRNA sequences by qRT-PCR. *TWEAK-shRNA-29* showed the highest efficiency. Data are presented as the mean ± SD (n=5). (**F**) Representative bright-field images showing cell morphology and myotube quantity in C2C12 cells (Scale bar = 50 μm). (**G**) Quantification of the number of myotubes. Data are presented as the mean ± SD (n=5). $^{*}P < 0.05$ vs Control group; $^{\#}P < 0.05$ vs PA group; $^{\wedge}P < 0.05$ vs DEX group; $^{\blacktriangledown}P < 0.05$ vs PrePA-Diff group; $^{\Delta}P < 0.05$ vs PrePA-Diff +NC group.


https://doi.org/10.2147/DMSO.S596507

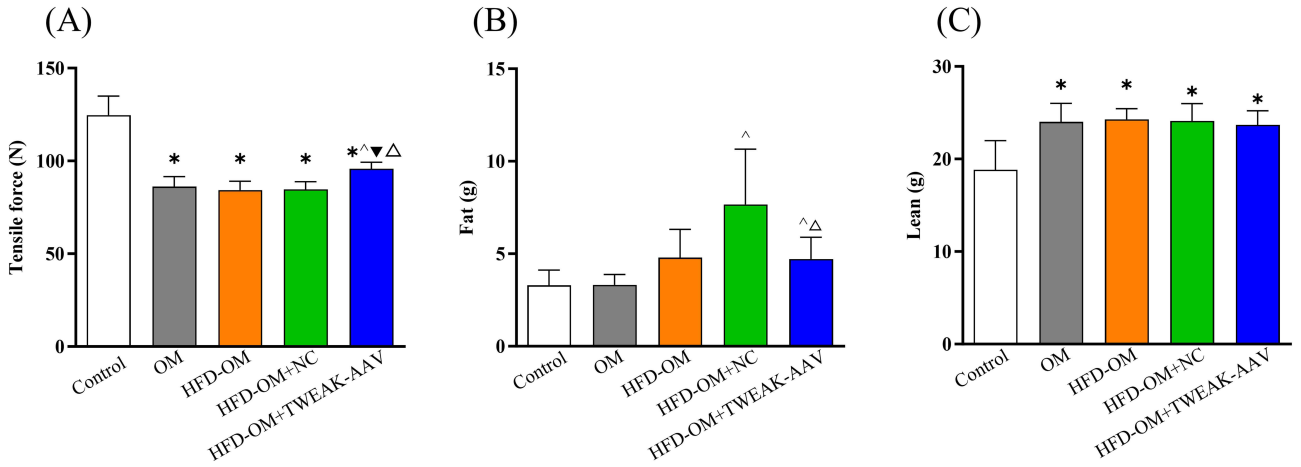


**Figure 2** The impact of *TWEAK* silencing on grip strength, fat mass, and lean mass in SO mice. (**A**) Measurement of forelimb grip strength in mice (n= 6). (**B**) Quantification of fat mass (g) measured by dual-energy X-ray absorptiometry (DEXA) (n= 6). (**C**) Quantification of lean mass (g) measured by DEXA (n = 6). Data are presented as the mean ± SD. **P* < 0.05 vs Control group; $^{\wedge}P$ < 0.05 vs OM group; $^{\blacktriangledown}P$ < 0.05 vs HFD-OM group; $^{\Delta}P$ < 0.05 vs HFD-OM+NC group.

the naturally larger body size of aged mice—no significant difference was observed between the HFD-OM+NC and HFD-OM+TWEAK-AAV groups (Figure 2C). Collectively, these results suggest that while TWEAK silencing may not significantly induce muscle hypertrophy (increase in lean mass) in the short term, it markedly improves muscle quality and function, as evidenced by enhanced grip strength and reduced fat accumulation. This dissociation between muscle mass and function highlights the critical role of skeletal muscle quality in SO recovery.

## TWEAK Silencing Attenuated Systemic Inflammation and Improved Lipid Profiles

In the in vitro experiments, the levels of TNF-α, IL-6, IL-1β, iNOS, TC, TG, HDL-C, and LDL-C were significantly higher in the PA, DEX, PrePA-Diff, PrePA-Diff+NC, and PrePA-Diff+TWEAK-shRNA groups compared to the control group. Furthermore, levels of these markers were generally higher in the PrePA-Diff group than in the PA and DEX groups, with the exception of TG levels, which were only significantly higher than those in the DEX group. However, TWEAK silencing reversed these trends; the PrePA-Diff+TWEAK-shRNA group exhibited significantly reduced levels of all aforementioned inflammatory and lipid indicators compared to the PrePA-Diff+NC group (Figure 3).

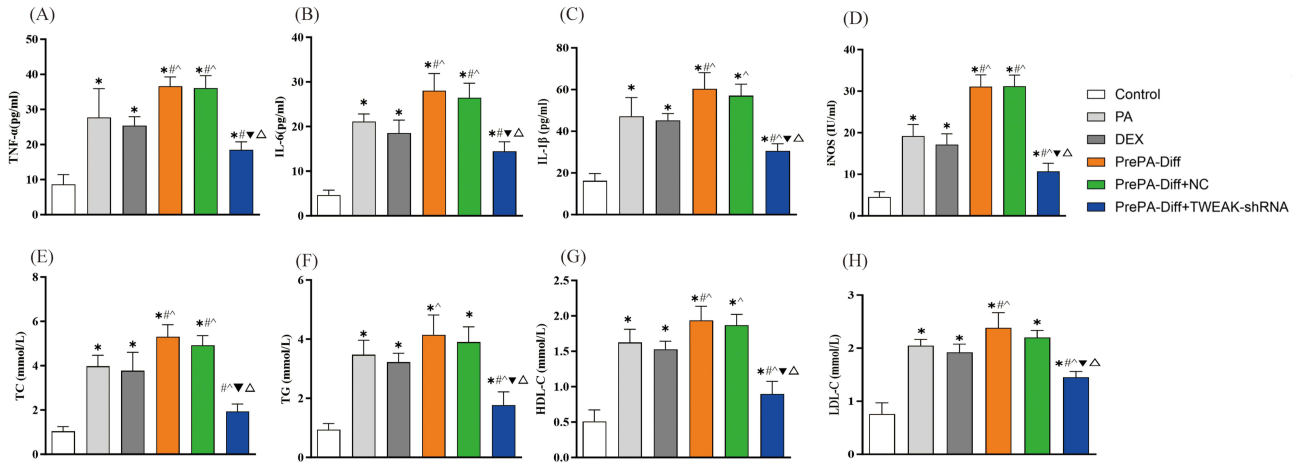


**Figure 3** Effects of TWEAK silencing on inflammatory cytokines and lipid profiles in the in vitro SO model. (**A**–**D**) The levels of inflammatory cytokines, including (**A**) TNF-α, (**B**) IL-6, (**C**) IL-1β, and (**D**) iNOS, were determined by ELISA. (**E**–**H**) Biochemical analysis of lipid levels, including (**E**) total cholesterol (TC), (**F**) triglycerides (TG), (**G**) HDL-C, and (**H**) LDL-C in C2C12 myotubes. Data are presented as the mean ± SD (n=6). **P* < 0.05 vs Control group; $^{\#}P$ < 0.05 vs PA group; $^{\wedge}P$ < 0.05 vs DEX group; $^{\blacktriangledown}P$ < 0.05 vs PrePA-Diff group; $^{\Delta}P$ < 0.05 vs PrePA-Diff+NC group.

 https://doi.org/10.2147/DMSO.S596507 

Furthermore, we conducted in vivo experiments to further explore the mechanisms underlying the protective effect of TWEAK inhibition on SO. Serum levels of TNF-α, IL-6, IL-1β, iNOS, TC, TG, HDL-C, and LDL-C were elevated in the OM, HFD-OM, HFD-OM+NC, and HFD-OM+TWEAK-AAV groups compared to the control group. When comparing the obesity models, the HFD-OM group exhibited significantly higher levels of all markers than the OM group. Similarly, in the HFD-OM+NC group, all indicators remained elevated compared to the OM group, with the exception of TNF-α. In contrast, silencing TWEAK significantly ameliorated these metabolic disturbances. Compared to the HFD-OM and HFD-OM+NC groups, the HFD-OM+TWEAK-AAV group exhibited significantly decreased serum levels of inflammatory cytokines (TNF-α, IL-6, IL-1β, and iNOS) and lipid profiles (TC, TG, LDL-C, and HDL-C) (Figure 4). These results demonstrate that inhibiting TWEAK can effectively improve systemic inflammation and lipid profiles in SO model mice.

## Silencing TWEAK Reduced Intracellular Calcium Accumulation in the SO Models

Excessive intracellular calcium accumulation can lead to ATP depletion and cytotoxicity. Using the calcium indicator Fluo-4 AM, we observed that intracellular calcium levels were significantly elevated in the PA, DEX, PrePA-Diff, PrePA-Diff+NC, and PrePA-Diff+TWEAK-shRNA groups compared to the control group. Notably, the PrePA-Diff group exhibited the highest calcium levels, significantly exceeding those in the PA and DEX groups. However, TWEAK silencing effectively mitigated this overload; the PrePA-Diff+TWEAK-shRNA group showed significantly reduced fluorescence intensity compared to the PrePA-Diff and PrePA-Diff+NC groups (Figure 5A).

## Silencing TWEAK Ameliorated Mitochondrial Dysfunction and Reduced Reactive Oxygen Species (ROS) Accumulation

ATP content and ROS levels are critical indicators of mitochondrial function. In the in vitro experiments, ATP levels were significantly reduced in the PA and DEX groups compared to the control group. Notably, the PrePA-Diff group exhibited the lowest ATP content, indicating severe mitochondrial impairment.[37] However, TWEAK inhibition reversed this deficit; the PrePA-Diff+TWEAK-shRNA group showed significantly higher ATP levels compared to both the PrePA-

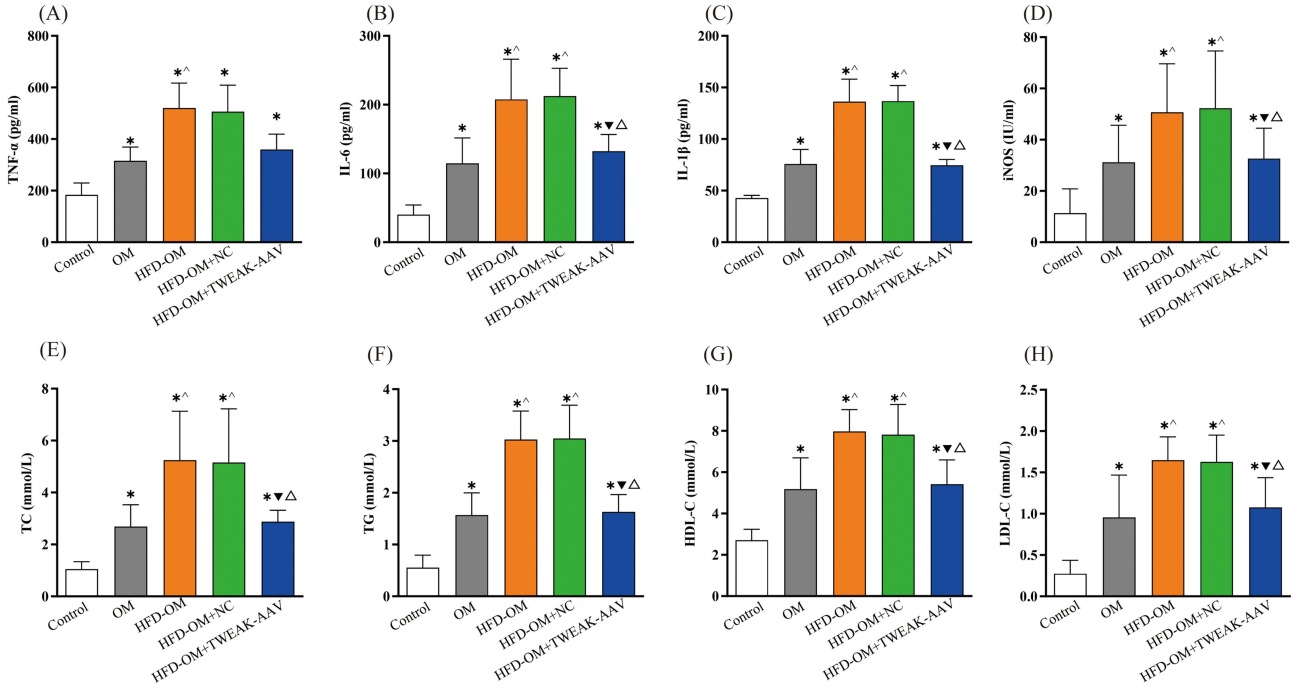


**Figure 4** Effects of TWEAK silencing on systemic inflammation and lipid profiles in SO mice. (**A**–**D**) Serum levels of inflammatory markers were determined by ELISA. Quantification of (**A**) TNF-α, (**B**) IL-6, (**C**) IL-1β, and (**D**) iNOS is shown. (**E**–**H**) Biochemical analysis of serum lipid profiles, including (**E**) Total Cholesterol (TC), (**F**) Triglycerides (TG), (**G**) HDL-C, and (**H**) LDL-C. Data are presented as the mean ± SD (n = 6). *$P < 0.05$ vs Control group; ^$P < 0.05$ vs OM group; ▼$P < 0.05$ vs HFD-OM group; △$P < 0.05$ vs HFD-OM+NC group.


https://doi.org/10.2147/DMSO.S596507

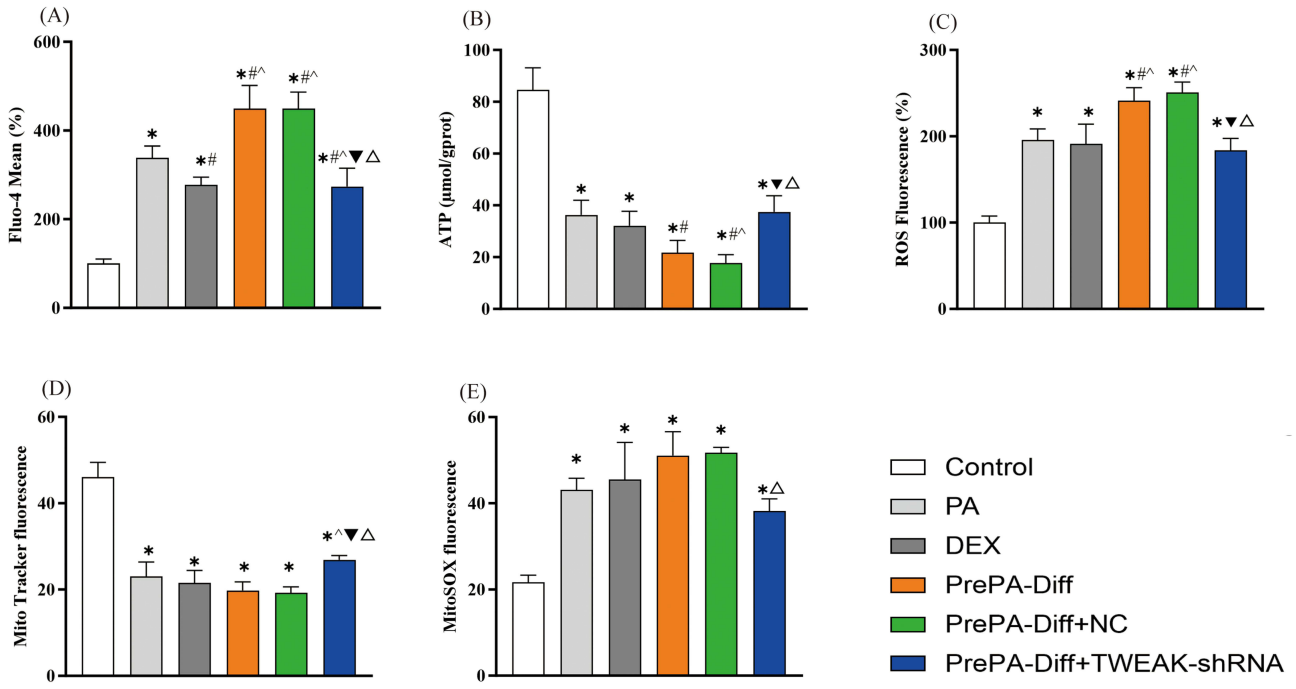


**Figure 5** TWEAK silencing attenuates calcium overload and mitochondrial dysfunction in the in vitro SO model. (**A**) Intracellular $Ca^{2+}$ levels were detected using the fluorescent indicator Fluo-4 AM. (**B** and **C**) Assessment of cellular energy metabolism and oxidative stress. (**B**) Intracellular ATP content and (**C**) intracellular ROS production. (**D** and **E**) Evaluation of mitochondrial status. (**D**) Mitochondrial mass (content) and (**E**) mitochondrial ROS levels. Data are presented as the mean ± SD (n = 3). $^{*}P < 0.05$ vs Control group; $^{\#}P < 0.05$ vs PA group; $^{\wedge}P < 0.05$ vs DEX group; $^{\blacktriangledown}P < 0.05$ vs PrePA-Diff group; $^{\triangle}P < 0.05$ vs PrePA-Diff+NC group.

Diff and PrePA-Diff+NC groups (Figure 5B). Conversely, ROS levels were significantly elevated in the PA, DEX, and PrePA-Diff groups. TWEAK-shRNA intervention significantly reduced these elevated ROS levels (Figure 5C). Furthermore, to evaluate mitochondrial integrity, we quantified mitochondrial mass and mitochondrial-specific ROS. Quantitative analysis showed significantly lower mitochondrial content in the PA, DEX, and PrePA-Diff groups (Figure 5D), while mitochondrial ROS levels were significantly higher in these groups than in the control (Figure 5E). Importantly, silencing TWEAK significantly attenuated the quantified levels of mitochondrial ROS and partially restored mitochondrial mass.

To visually validate these results, we performed fluorescence microscopy. As shown in Figure 6A, the fluorescence intensity of MitoTracker Red (indicating mitochondrial mass) was markedly reduced in the PA, DEX, and PrePA-Diff groups compared to the control. Consistent with the quantification, the recovered red fluorescence in the PrePA-Diff +TWEAK-shRNA group evidenced the restoration of mitochondrial mass. Regarding oxidative stress, MitoSOX staining (Figure 6B) revealed intense red fluorescence (indicating high mitochondrial ROS) in the PrePA-Diff group, which was significantly attenuated by TWEAK silencing. These results suggest that TWEAK inhibition promotes the restoration of mitochondrial homeostasis.

Consistent with the in vitro findings, in vivo analysis of gastrocnemius muscle tissue revealed elevated intracellular calcium levels in the OM, HFD-OM, HFD-OM+NC, and HFD-OM+TWEAK-AAV groups compared to the control group. The HFD-OM group showed a further increase in calcium accumulation compared to the OM group. Importantly, TWEAK inhibition significantly attenuated this increase; the HFD-OM+TWEAK-AAV group displayed significantly lower calcium levels compared to the HFD-OM and HFD-OM+NC groups (Figure 7A). These findings were corroborated by in vivo mitochondrial experiments. Compared to the control group, ATP levels were significantly reduced, while ROS levels were markedly elevated in all model groups (OM, HFD-OM, and HFD-OM+NC). Specifically, the HFD-OM group exhibited a further deterioration in mitochondrial function, characterized by lower ATP and higher ROS levels compared to the OM group. Notably, silencing TWEAK reversed these trends: the HFD-OM+TWEAK-AAV group showed significantly increased ATP levels (Figure 7B) and decreased ROS accumulation (Figure 7C) compared to the

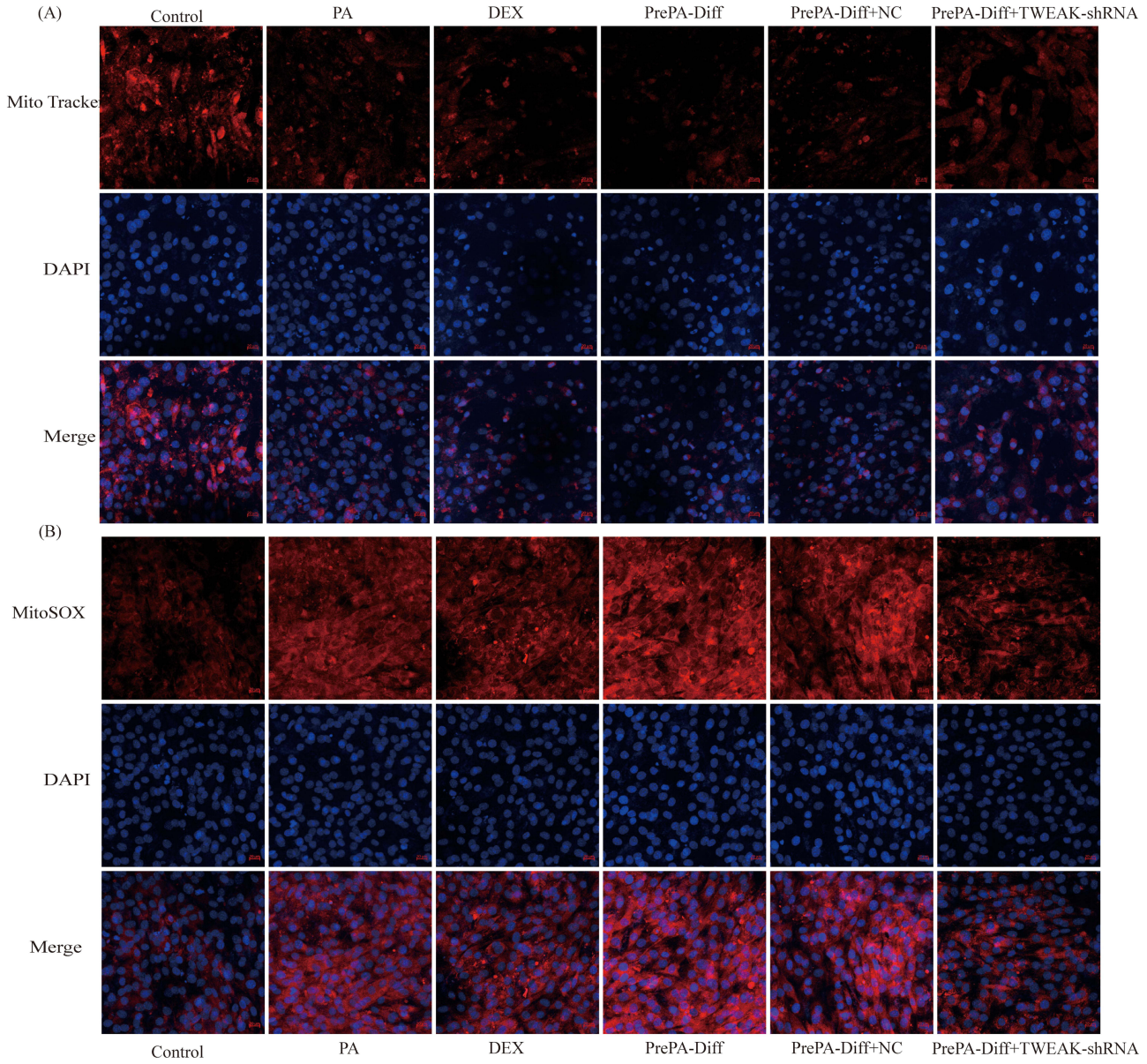


**Figure 6** Representative confocal microscopy images of mitochondrial content and mitochondrial ROS. (**A**) Visualization of mitochondrial content using the MitoTracker Red probe. (**B**) Detection of mitochondrial ROS generation using the MitoSOX Red indicator. Images are representative of 3 independent experiments (n = 3). Scale bar = 20 μm.

HFD-OM and HFD-OM+NC groups. These data demonstrate that inhibiting TWEAK can partially restore ATP metabolism and alleviate oxidative stress.

## TWEAK Silencing Promoted Mitochondrial Biogenesis via the AMPK/SIRT1/PGC-1α Signaling Pathway

Impaired mitochondrial biogenesis acts as a key driver of SO. TWEAK/Fn14 signaling is known to negatively regulate this process. To investigate the molecular mechanism, we first verified the in vivo knockdown efficiency at the mRNA level. qRT-PCR results showed that TWEAK (Figure 7D) and Fn14 (Figure 7E) mRNA levels were significantly reduced in the HFD-OM+TWEAK-AAV group compared to the NC group. Similarly, in the in vitro models, TWEAK and Fn14 mRNA levels were significantly reduced in the PrePA-Diff+TWEAK-shRNA group compared to the NC group (Figure 8).


https://doi.org/10.2147/DMSO.S596507

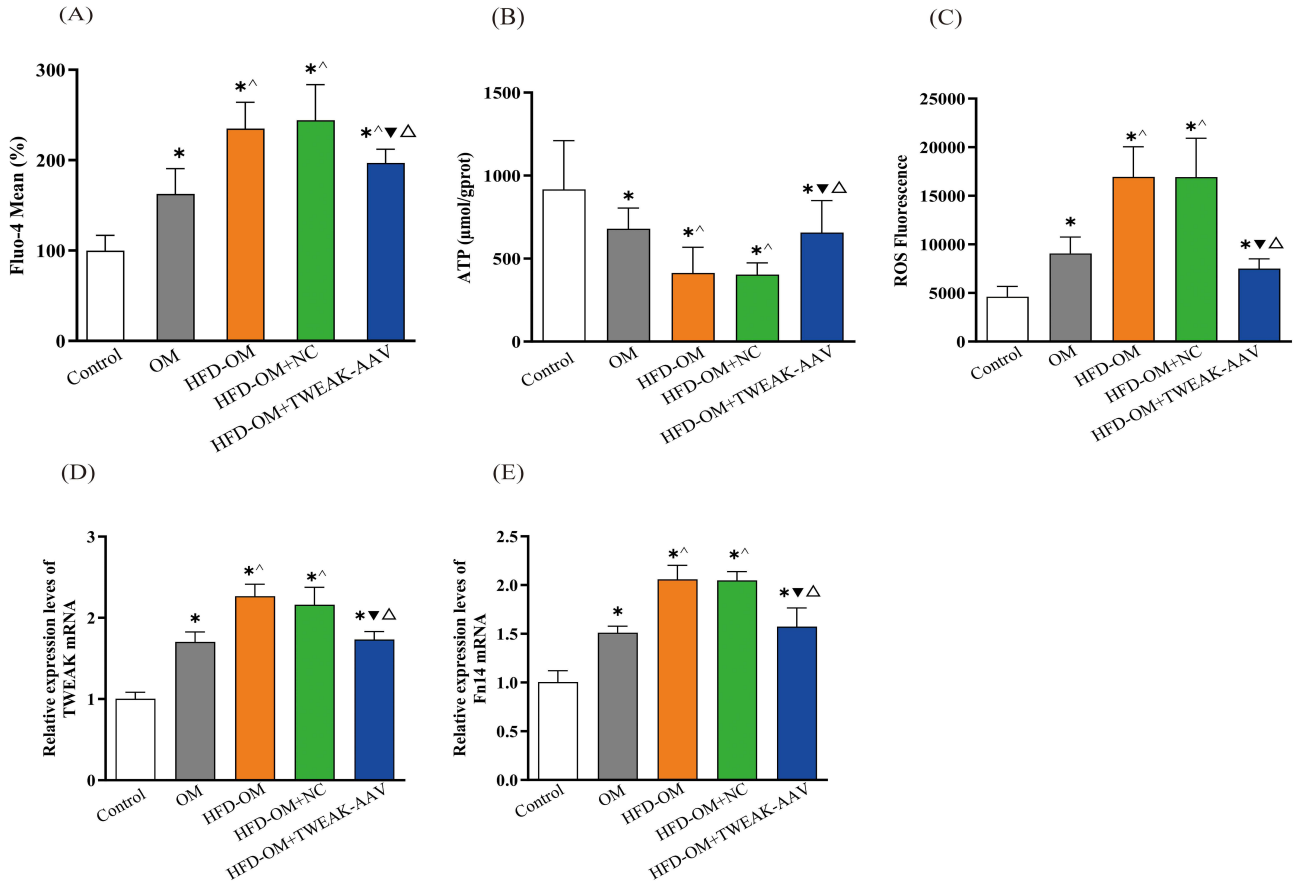


**Figure 7** Effects of TWEAK silencing on intracellular calcium, ATP production, and oxidative stress in SO mice. (**A**) Intracellular Ca2+ levels were assessed using the Ca2+ indicator dye Fluo-4 AM. (**B** and **C**) Assessment of mitochondrial function indicators in gastrocnemius muscle tissue, including (**B**) ATP content and (**C**) ROS levels. (**D** and **E**) Relative mRNA expression levels of (**D**) TWEAK and (**E**) Fn14 were determined by qRT-PCR. Data are presented as the mean ± SD (n= 6). **P* < 0.05 vs Control group; ^*P* < 0.05 vs OM group; ▼*P* < 0.05 vs HFD-OM group; △*P* < 0.05 vs HFD-OM+NC group. (Statistical significance was determined by one-way ANOVA).

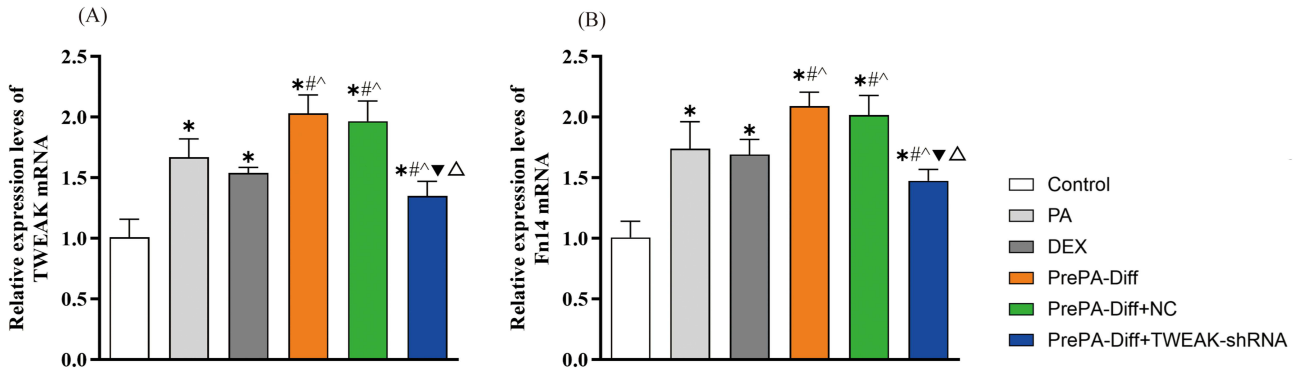


**Figure 8** Effect of TWEAK silencing on *TWEAK* and *Fn14* mRNA expression in an in vitro SO model. Relative mRNA levels were determined by qRT-PCR. The graphs show the expression levels of (**A**) *TWEAK* and (**B**) *Fn14*. Data are presented as the mean ± SD (n = 5). **P* < 0.05 vs Control group; #*P* < 0.05 vs PA group; ^*P* < 0.05 vs DEX group; ▼*P* < 0.05 vs PrePA-Diff group; △*P* < 0.05 vs PrePA-Diff+NC group. (Statistical significance was analyzed by one-way ANOVA).

We next examined the protein expression of key components in the mitochondrial biogenesis pathway using Western blotting. In the in vitro models, the expression levels of TWEAK, Fn14, and phosphorylated p38 (p-p38) were significantly upregulated in the PA, DEX, and PrePA-Diff groups compared to the control. Conversely, the key biogenesis regulators—phosphorylated AMPK (p-AMPK), SIRT1, and PGC-1α were significantly downregulated. However, TWEAK silencing effectively reversed these alterations: the PrePA-Diff+TWEAK-shRNA group exhibited downregulated TWEAK, Fn14, and

p-p38 levels, while significantly restoring p-AMPK, SIRT1, and PGC-1α levels compared to the PrePA-Diff+NC group (Figures 9 and 10). Crucially, no significant differences were observed in the total protein levels of AMPK and p38 in vitro (Figures 9 and 10). The significant upregulation of p-AMPK in the absence of changes in total AMPK indicates a robust activation of AMPK signaling activity by TWEAK silencing, rather than an alteration in the total protein pool.

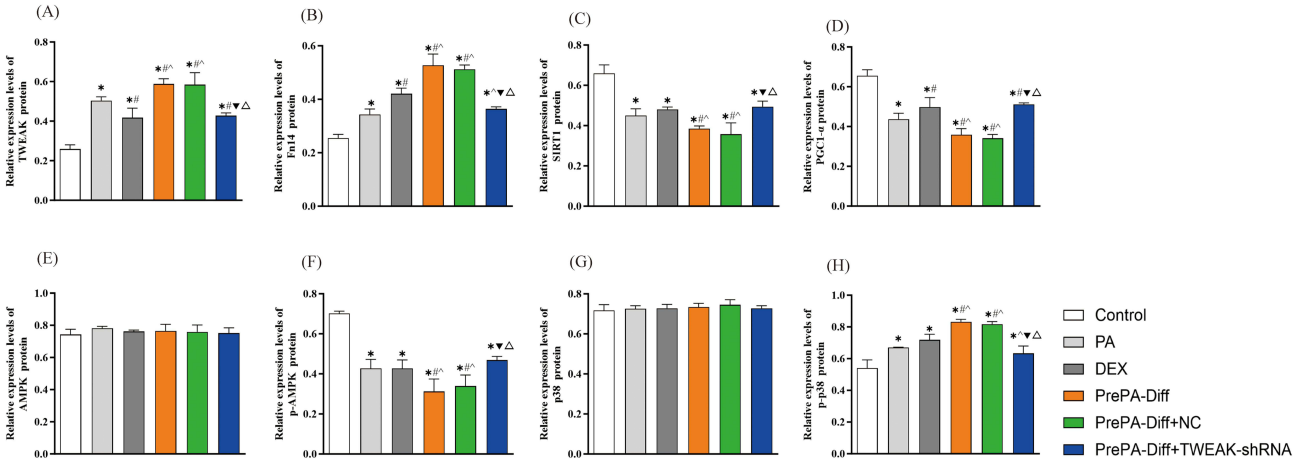


**Figure 9** Quantitative analysis of the TWEAK/Fn14 axis and downstream signaling pathways in the in vitro SO model. Relative protein expression levels were determined by Western blotting. The bar charts represent the relative expression of (**A**) TWEAK, (**B**) Fn14, (**C**) SIRT1, (**D**) PGC-1α, (**E**) total AMPK, (**F**) p-AMPK, (**G**) total p38, and (**H**) p-p38. Data are presented as the mean ± SD from three independent experiments (n = 3). $^{*}P < 0.05$ vs Control group; $^{\#}P < 0.05$ vs PA group; $^{\wedge}P < 0.05$ vs DEX group; $^{\blacktriangledown}P < 0.05$ vs PrePA-Diff group; $^{\triangle}P < 0.05$ vs PrePA-Diff+NC group.

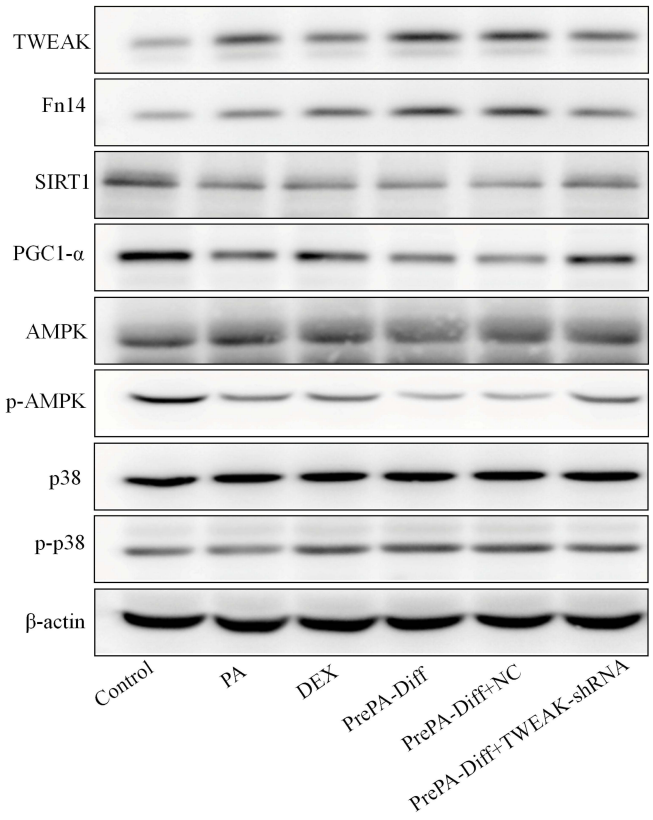


**Figure 10** Representative Western blot images of the TWEAK/Fn14 axis and downstream signaling proteins. Representative protein bands for TWEAK, Fn14, SIRT1, PGC-1α, AMPK, p-AMPK, p38, and p-p38 are shown. β-actin was used as the internal loading control. The quantitative analysis of these bands is presented in Figure 9.


https://doi.org/10.2147/DMSO.S596507

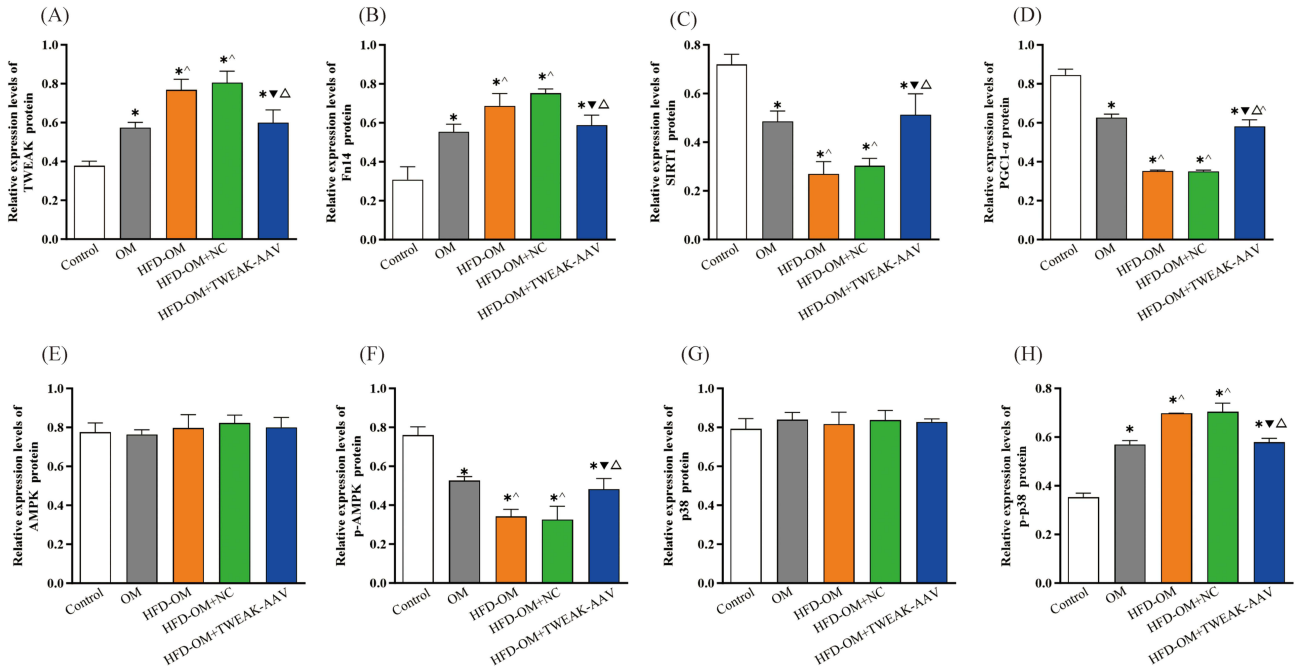


**Figure 11** Effect of TWEAK inhibition on the AMPK/SIRT1/PGC-1α signaling pathway in the in vivo SO model. Relative protein expression levels were determined by Western blotting. The quantitative analysis shows the expression of (**A**) TWEAK, (**B**) Fn14, (**C**) SIRT1, (**D**) PGC-1α, (**E**) total AMPK, (**F**) p-AMPK, (**G**) total p38, and (**H**) p-p38. Data are presented as the mean ± SD (n = 3). Statistical significance was determined by one-way ANOVA followed by Tukey's post hoc test. **P* < 0.05 vs Control group; ^*P* < 0.05 vs OM group; ▼*P* < 0.05 vs HFD-OM group; △*P* < 0.05 vs HFD-OM+NC group.

These findings were consistently reproduced in the SO mouse model. Compared to the control group, the OM and HFD-OM groups showed suppressed levels of SIRT1, PGC-1α, and p-AMPK, alongside elevated levels of TWEAK, Fn14, and p-p38. Notably, the HFD-OM group displayed a more severe inhibition of the AMPK/SIRT1 pathway and higher expression of TWEAK pathway components compared to the OM group. Importantly, TWEAK inhibition via AAV significantly reactivated this pathway, increasing SIRT1, PGC-1α, and p-AMPK expression while suppressing p-p38, TWEAK, and Fn14 levels in the HFD-OM+TWEAK-AAV group compared to the HFD-OM+NC group (Figures 11 and 12). Consistent with the in vitro data, total AMPK and p38 levels remained unchanged across all in vivo groups (Figures 11 and 12). This phosphorylation-driven activation is consistent with the initiation of the PGC-1α-mediated mitochondrial biogenesis program.

## Discussion

In the present study, we provide evidence that inhibition of TWEAK/Fn14 effectively attenuates SO by restoring mitochondrial biogenesis via the AMPK/SIRT1/PGC-1α signaling axis. Given that SO is not merely the co-occurrence of muscle atrophy and obesity but a synergistic condition driven by lipotoxicity and inflammation, appropriate experimental models are crucial for elucidating its pathogenesis. To this end, we utilized a "PrePA-Diff" in vitro model adapted from Nguyen et al,[32] which specifically mimics the lipid-accumulated microenvironment surrounding muscle satellite cells. Unlike standard atrophy models, exposing myoblasts to palmitate (PA) prior to differentiation better recapitulates the impairment of regenerative capacity observed in obese skeletal muscle.[38] Consistent with the elevated inflammatory profile seen in clinical SO patients, we observed significantly upregulated TWEAK levels in our models. Our data indicate that this lipotoxic environment suppresses myogenic regulators (eg, MyoD), and importantly, we demonstrate that blocking the TWEAK/Fn14 axis can ameliorate these deficits, effectively rescuing myotube formation even under high-fat conditions.

In terms of physiological outcomes, our in vivo results revealed a distinct improvement in muscle function following TWEAK inhibition. Specifically, silencing TWEAK reduced fat content and significantly increased handgrip strength in SO mice. Notably, the improvement in muscle strength appeared more pronounced than the changes in muscle mass. This discrepancy points to an enhancement in "muscle quality" rather than solely "muscle quantity." Muscle quality is closely

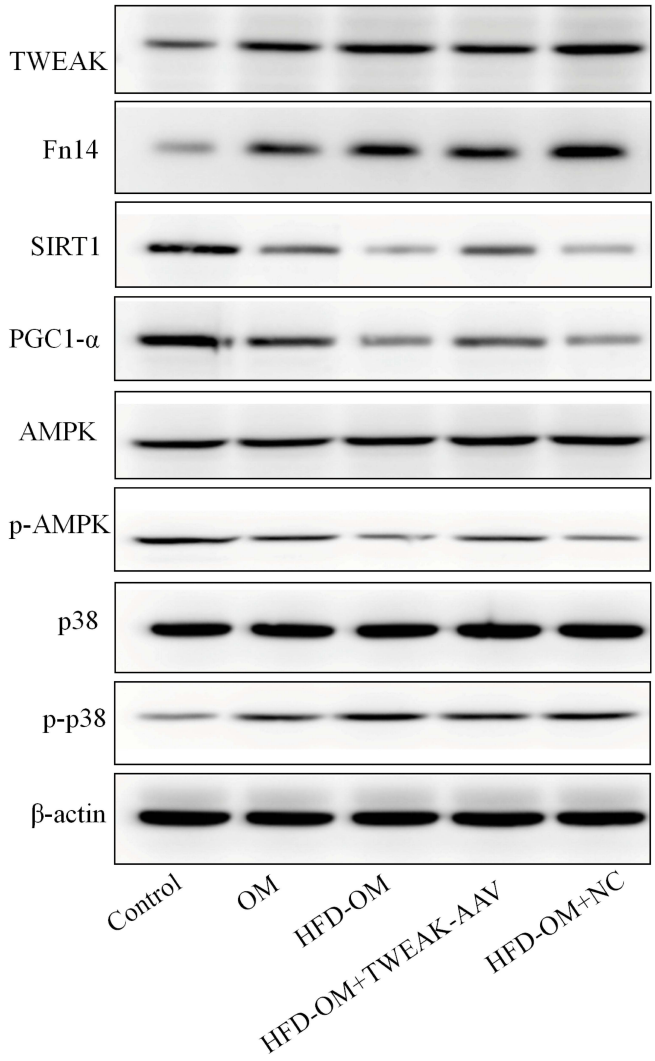


**Figure 12** Representative Western blot images of the TWEAK/Fn14 axis and downstream signaling proteins in the in vivo model. Representative protein bands for TWEAK, Fn14, SIRT1, PGC-1α, AMPK, p-AMPK, p38, and p-p38 are shown. β-actin was used as the internal loading control. The quantitative analysis of these bands is presented in Figure 11.

linked to mitochondrial bioenergetics.[39] Beyond merely supplying the basal ATP required for actomyosin cross-bridge cycling, intact mitochondrial networks are indispensable for sustaining oxidative phosphorylation and maintaining intracellular $NAD^+$ homeostasis, both of which are fundamental bioenergetic prerequisites for maximal force generation.[40] We found that TWEAK inhibition significantly enhanced mitochondrial content and ATP production while suppressing ROS generation in both in vitro and in vivo models. This suggests that the restoration of grip strength is driven by these profound improvements in mitochondrial efficiency and energy supply, rather than simple hypertrophy. Mechanistically, this protective effect appears to be mediated by the re-activation of the AMPK/SIRT1/PGC-1α pathway. While previous studies have shown that TWEAK suppresses PGC-1α,[41] our data further elucidate that TWEAK inhibition specifically upregulates the phosphorylation of AMPK (p-AMPK) and SIRT1 expression, thereby rescuing the downstream mitochondrial biogenesis machinery. Furthermore, we observed that TWEAK inhibition reduced intracellular calcium influx. Since calcium overload is a known trigger for proteolysis and apoptosis in wasting muscle,[42] this reduction likely serves as a complementary protective mechanism, contributing to the preservation of sarcolemmal integrity.

Our findings regarding the TWEAK/Fn14 axis align with and extend the existing literature on muscle pathophysiology. As highlighted in our Introduction, while previous epidemiological and transcriptomic studies have largely established a correlative link between elevated TWEAK levels and age-related metabolic decline, our study provides crucial causal

 https://doi.org/10.2147/DMSO.S596507 

evidence in vivo. It is well-established that TWEAK acts as a potent inhibitor of myogenesis. Previous studies utilizing Fn14-Fc chimeras or TWEAK-knockout models have demonstrated that neutralizing TWEAK enhances myogenic differentiation and myotube formation.[25,43] Beyond muscle regeneration, our study highlights the critical role of TWEAK in perpetuating the inflammatory loop characteristic of SO. TWEAK is known to stimulate chemokine expression in mesenchymal progenitors and create a pro-inflammatory microenvironment.[44,45] In the context of obesity, elevated TWEAK/Fn14 levels in adipose tissue have been linked to maladaptive remodeling and systemic metabolic complications.[46,47] Furthermore, transgenic overexpression of TWEAK in skeletal muscle has been shown to induce insulin resistance and suppress whole-body metabolism.[30] Uniquely, our data bridge these two pathological domains—sarcopenia and obesity. We observed that silencing TWEAK not only reduced inflammatory markers but also exerted a dual beneficial effect: decreasing fat mass while enhancing muscle function. These observations suggest that targeting TWEAK may not merely treat muscle atrophy or obesity in isolation but disrupts the synergistic "vicious cycle" of metabolic inflammation that drives SO.

The restoration of mitochondrial function observed in our study is mechanically underpinned by the AMPK/SIRT1/PGC-1α signaling cascade. PGC-1α is considered a master regulator of mitochondrial biogenesis,[17] and its expression is critical for maintaining oxidative muscle fibers. Our results support a model where TWEAK acts as a molecular "brake" on this energy-sensing pathway. Under SO conditions, TWEAK-mediated suppression of PGC-1α exacerbates mitochondrial dysfunction. We demonstrate that TWEAK inhibition releases this brake, effectively re-activating AMPK phosphorylation. It is worth noting that while the total protein expression of AMPK remained unchanged, the specific increase in its phosphorylated form (p-AMPK) indicates a functional activation of the kinase. As a key energy sensor, activated AMPK triggers mitochondrial biogenesis and activates SIRT1, which in turn deacetylates and activates PGC-1α.[48] By restoring this axis, TWEAK inhibition helps reverse the bioenergetic deficit of SO, promoting a shift in the muscle phenotype from a catabolic, inflammatory state to a more anabolic, oxidative state.

From a clinical perspective, the therapeutic potential of TWEAK inhibition is significant. Epidemiological data indicate that the cardiometabolic multimorbidity risk of SO exceeds those of sarcopenia or obesity alone.[49] Current interventions often fail to address both components simultaneously; for instance, caloric restriction for obesity may inadvertently exacerbate muscle loss.[50] Our findings suggest that the TWEAK/Fn14 axis represents a viable target for integrated intervention. However, it is imperative to acknowledge the inherent mechanistic complexity of SO. As established in the literature, SO is not driven by a single pathway, but rather by an intricate, multifactorial network involving aging, ectopic fat deposition (lipotoxicity), and dysfunctional endocrine crosstalk between adipose and skeletal muscle tissues.[51] Indeed, our recent multiomics and Mendelian randomization analyses have further reinforced that immune-metabolic dysregulation acts as a core, causal bridge driving the pathogenesis of both muscle wasting and adiposity.[52]

Within this complex, immune-driven landscape, TWEAK occupies a uniquely advantageous therapeutic position. Conventional single-target therapies, such as myostatin inhibitors, primarily increase muscle mass but frequently fail to translate into clinically relevant improvements in physical performance.[53] In contrast, pharmacological inhibition of the TWEAK/Fn14 pathway operates further upstream. It uniquely uncouples systemic pro-inflammatory signals from local metabolic deterioration, offering a dual-pronged approach to simultaneously rescue mitochondrial bioenergetics and systemic homeostasis. Recent studies have robustly established this axis as a central orchestrator of both skeletal muscle remodeling and systemic metabolism. For instance, Meijboom et al demonstrated that dysregulation of the TWEAK/Fn14 pathway deeply impacts myopathy, myogenesis, and glucose metabolism in neuromuscular disorders.[54] Crucially, the pharmacological feasibility and clinical safety of targeting this axis have already been corroborated in human trials. BIIB023, a neutralizing humanized monoclonal antibody against TWEAK, has successfully completed Phase 1 clinical evaluations. In patients with rheumatoid arthritis—a condition characterized by chronic systemic inflammation similar to SO—BIIB023 exhibited a highly favorable safety and tolerability profile, effectively suppressing serum-soluble TWEAK levels and promoting downward trends in pro-inflammatory biomarkers such as MCP-1 and IP-10.[34] Furthermore, subsequent analyses confirmed that BIIB023 demonstrates stable target engagement and consistent safety profiles across diverse populations, including Chinese, Japanese, and Caucasian cohorts.[55] Given that SO is driven by shared inflammatory crosstalk and metabolic dysfunction, repurposing existing, clinically-tested anti-TWEAK neutralizing antibodies presents a highly translational therapeutic strategy. Such pharmacological strategies could potentially be combined with exercise regimens to synergistically amplify mitochondrial biogenesis, thereby extending healthspan in aging populations.

Despite these promising findings, several limitations of the current study must be acknowledged. First, while we confirmed the efficacy of AAV-mediated TWEAK silencing in muscle, potential off-target effects in other metabolically active organs (eg, liver) cannot be fully ruled out, as systemic leakage of AAV vectors has been documented to transduce hepatocytes.[56] This warrants future tissue-specific biodistribution studies. Second, our analysis focused on endpoint therapeutic efficacy. Consequently, we did not capture the dynamic fluctuations of TWEAK mRNA and protein expression during the progressive development of SO. Future investigations utilizing multi-timepoint profiling would be beneficial to map the temporal window for optimal intervention. Third, to precisely navigate the translational journey from our preclinical murine model to future human therapies, a step-wise clinical approach is necessary. Although the safety of anti-TWEAK monoclonal antibodies (eg, BIIB023) has been validated in Phase 1 human trials for other inflammatory diseases, future efforts must pivot to Phase II proof-of-concept trials specifically designed for older adults with sarcopenic obesity. These upcoming translational studies must rigorously evaluate optimal dosing regimens, therapeutic time windows, and potential synergistic effects when pharmacotherapy is combined with standard-of-care lifestyle interventions, such as resistance exercise and nutritional supplementation.[57,58] Finally, we acknowledge that the sample sizes used in our current study (n=3–5 for in vitro experiments and n=6–8 for animal cohorts) are relatively small. Although statistically significant differences were achieved and the results were highly consistent across multiple independent assays, small sample sizes can potentially limit the overall statistical power and the generalizability of the findings. Specifically, they may increase the risk of overestimating effect sizes or type II errors. Therefore, while our data provide a solid foundational proof-of-concept, future studies incorporating larger sample sizes and broader experimental models are warranted to further validate the robustness and clinical translatability of these mechanisms. In conclusion, notwithstanding these limitations, our study identifies the TWEAK/Fn14 axis as a pivotal molecular brake on mitochondrial function in sarcopenic obesity, providing a compelling rationale for its therapeutic targeting to reverse age-related musculoskeletal and metabolic decline.

## Conclusion

In summary, our study highlights the pivotal role of the TWEAK/Fn14 signaling pathway in the pathogenesis of sarcopenic obesity. We provide compelling in vitro and in vivo evidence that TWEAK inhibition rescues muscle function and metabolic homeostasis by restoring mitochondrial biogenesis via the AMPK/SIRT1/PGC-1α axis (Figure 13). While

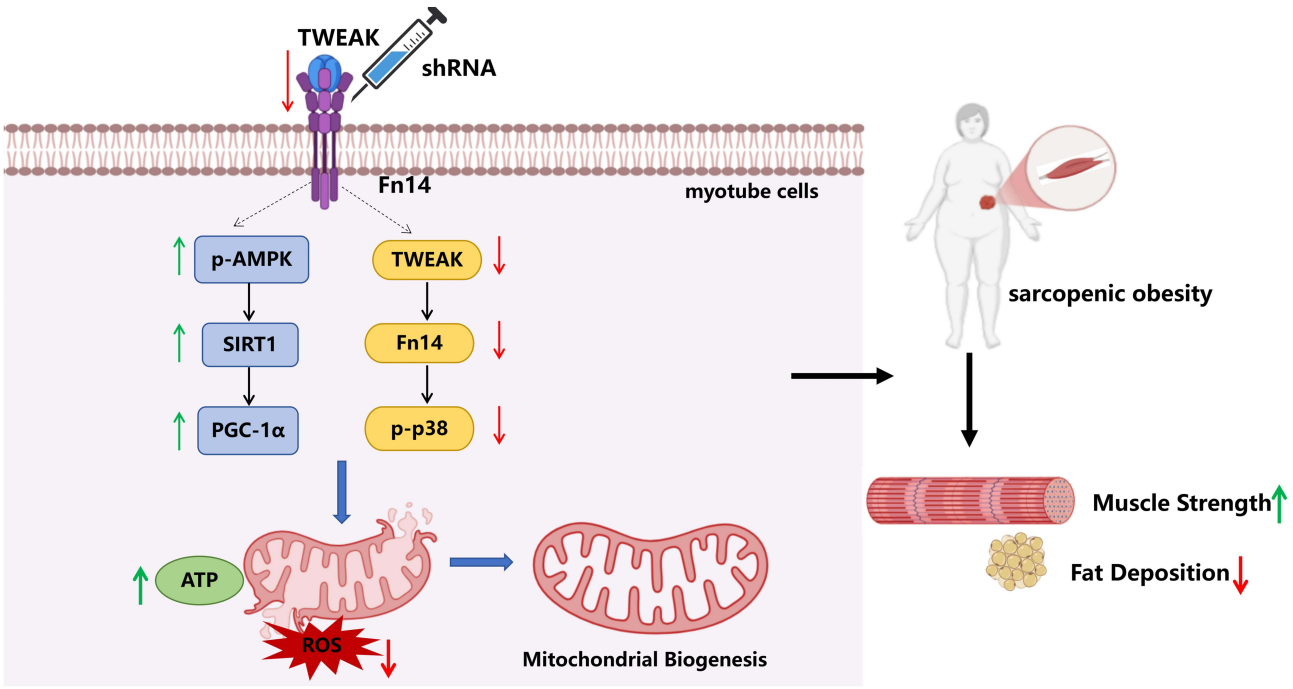


**Figure 13** Schematic diagram illustrating the mechanism by which TWEAK/Fn14 inhibition alleviates sarcopenic obesity via the AMPK/SIRT1/PGC-1α signaling pathway. Under HFD and OM conditions (or in the SO model), elevated TWEAK binds to Fn14, activating p38 MAPK and subsequently inhibiting the AMPK/SIRT1/PGC-1α pathway. This leads to reduced mitochondrial biogenesis and ATP synthesis, contributing to sarcopenic obesity. However, inhibition of TWEAK (eg, via TWEAK-AAV) restores AMPK phosphorylation, upregulates SIRT1 and PGC-1α, thereby promoting mitochondrial function and ameliorating muscle loss and fat accumulation.


https://doi.org/10.2147/DMSO.S596507

further research is needed to fully elucidate the temporal dynamics and systemic safety profile, these findings establish the TWEAK/Fn14 pathway as a highly translational therapeutic target for combating age-related musculoskeletal and metabolic decline.

## Data Sharing Statement

The datasets used and/or analyzed during the current study are available from the corresponding author on reasonable request.

## Ethics Approval

All animal care and experimental procedures were performed in accordance with the National Standard of the People's Republic of China (GB/T 42011-2022: Laboratory animals-General code of animal welfare). The experimental protocols were approved by the Experimental Animal Ethics and Welfare Committee of the People's Hospital of Xinjiang Uygur Autonomous Region (reference number: KY2021031726). The reporting of this study is in accordance with the ARRIVE guidelines.

## Acknowledgments

We thank Medjaden Inc. for its assistance in the preparation of this paper.

## Author Contributions

Saiyare Xuekelati and Zhuoya Maimaitiwusiman: Conceptualization, Data curation, and Writing – original draft. Shuke Guo and Qihong Xu: Investigation, Visualization, and Writing – review & editing. Jiayu Ke and Lei Xu: Methodology, Validation, and Writing – review & editing. Yining Yang: Conceptualization (lead), Supervision, Resources, and Writing – review & editing. Yanying Guo: Conceptualization, Methodology, Supervision, and Writing – review & editing. Hongmei Wang: Project administration, Conceptualization, and Writing – review & editing. All authors gave final approval of the version to be published; have agreed on the journal to which the article has been submitted; and agree to be accountable for all aspects of the work.

## Funding

This work was supported by the National Natural Science Foundation of China (82160276), Key Project of the Natural Science Foundation of Xinjiang Uygur Autonomous Region (2025D01D30), Natural Science Foundation of Xinjiang Uygur Autonomous Region (2023D01C77) and Health Care Research Special Project of Xinjiang Uygur Autonomous Region (BL202504).

## Disclosure

The authors declare that they have no conflict of interest.

## References

1. Cruz-Jentoft AJ, Sayer AA. Sarcopenia. *Lancet*. 2019;393:2636–2646.
2. Shafiee G, Keshtkar A, Soltani A, et al. Prevalence of sarcopenia in the world: a systematic review and meta-analysis of general population studies. *J Diabetes Metab Disord*. 2017;16:21.
3. Petermann-Rocha F, Balntzi V, Gray SR, et al. Global prevalence of sarcopenia and severe sarcopenia: a systematic review and meta-analysis. *J Cachexia Sarcopenia Muscle*. 2022;13:86–99. doi:10.1002/jcsm.12783
4. Gallagher D, Ruts E, Visser M, et al. Weight stability masks sarcopenia in elderly men and women. *Am J Physiol Endocrinol Metab*. 2000;279:E366–375. doi:10.1152/ajpendo.2000.279.2.E366
5. Donini LM, Busetto L, Bischoff SC, et al. Definition and diagnostic criteria for sarcopenic obesity: ESPEN and EASO consensus statement. *Obes Facts*. 2022;15:321–335. doi:10.1159/000521241
6. Gao Q, Mei F, Shang Y, et al. Global prevalence of sarcopenic obesity in older adults: a systematic review and meta-analysis. *Clin Nutr*. 2021;40:4633–4641. doi:10.1016/j.clnu.2021.06.009
7. Kalinkovich A, Livshits G. Sarcopenic obesity or obese sarcopenia: a cross talk between age-associated adipose tissue and skeletal muscle inflammation as a main mechanism of the pathogenesis. *Ageing Res Rev*. 2017;35:200–221. doi:10.1016/j.arr.2016.09.008
8. Bellanti F, Lo Buglio A, Vendemiale G. Mitochondrial impairment in sarcopenia. *Biology*. 2021;10:10031. doi:10.3390/biology10010031
9. Huang Y, Zhu X, Chen K, et al. Resveratrol prevents sarcopenic obesity by reversing mitochondrial dysfunction and oxidative stress via the PKA/LKB1/AMPK pathway. *Aging*. 2019;11:2217–2240. doi:10.18632/aging.101910

10. Arany Z. PGC-1 coactivators and skeletal muscle adaptations in health and disease. *Curr Opin Genet Dev*. 2008;18:426–434. doi:10.1016/j.gde.2008.07.018
11. Finck BN, Kelly DP. PGC-1 coactivators: inducible regulators of energy metabolism in health and disease. *J Clin Invest*. 2006;116:615–622. doi:10.1172/JCI27794
12. Scarpulla RC. Metabolic control of mitochondrial biogenesis through the PGC-1 family regulatory network. *Biochim Biophys Acta*. 2011;1813:1269–1278. doi:10.1016/j.bbamcr.2010.09.019
13. Islam H, Edgett BA, Gurd BJ. Coordination of mitochondrial biogenesis by PGC-1α in human skeletal muscle: a re-evaluation. *Metabolism*. 2018;79:42–51.
14. Lin J, Wu H, Tarr PT, et al. Transcriptional co-activator PGC-1 alpha drives the formation of slow-twitch muscle fibres. *Nature*. 2002;418:797–801.
15. Wende AR, Schaeffer PJ, Parker GJ, et al. A role for the transcriptional coactivator PGC-1alpha in muscle refueling. *J Biol Chem*. 2007;282:36642–36651. doi:10.1074/jbc.M707006200
16. Sczelecki S, Besse-Patin A, Abboud A, et al. Loss of PGC-1α expression in aging mouse muscle potentiates glucose intolerance and systemic inflammation. *Am J Physiol Endocrinol Metab*. 2014;306:E157–167. doi:10.1152/ajpendo.00578.2013
17. Islam H, Hood DA, Gurd BJ. Looking beyond PGC-1α: emerging regulators of exercise-induced skeletal muscle mitochondrial biogenesis and their activation by dietary compounds. *Appl Physiol Nutr Metab*. 2020;45:11–23. doi:10.1139/apnm-2019-0069
18. Geng J, Wei M, Yuan X, et al. TIGAR regulates mitochondrial functions through SIRT1-PGC1α pathway and translocation of TIGAR into mitochondria in skeletal muscle. *FASEB J*. 2019;33:6082–6098. doi:10.1096/fj.201802209R
19. Price NL, Gomes AP, Ling AJ, et al. SIRT1 is required for AMPK activation and the beneficial effects of resveratrol on mitochondrial function. *Cell Metab*. 2012;15:675–690.
20. Mohamed JS, Hajira A, Pardo PS, et al. MicroRNA-149 inhibits PARP-2 and promotes mitochondrial biogenesis via SIRT-1/PGC-1α network in skeletal muscle. *Diabetes*. 2014;63:1546–1559.
21. Gurd BJ. Deacetylation of PGC-1α by SIRT1: importance for skeletal muscle function and exercise-induced mitochondrial biogenesis. *Appl Physiol Nutr Metab*. 2011;36:589–597.
22. Hood DA, Memme JM, Oliveira AN, et al. Maintenance of skeletal muscle mitochondria in health, exercise, and aging. *Annu Rev Physiol*. 2019;81:19–41.
23. Cantó C, Auwerx J. PGC-1alpha, SIRT1 and AMPK, an energy sensing network that controls energy expenditure. *Curr Opin Lipidol*. 2009;20:98–105. doi:10.1097/MOL.0b013e328328d0a4
24. Steinberg GR, Michell BJ, van Denderen BJ, et al. Tumor necrosis factor alpha-induced skeletal muscle insulin resistance involves suppression of AMP-kinase signaling. *Cell Metab*. 2006;4(6):465–474. doi:10.1016/j.cmet.2006.11.005
25. Mittal A, Bhatnagar S, Kumar A, et al. Genetic ablation of TWEAK augments regeneration and post-injury growth of skeletal muscle in mice. *Am J Pathol*. 2010;177:1732–1742. doi:10.2353/ajpath.2010.100335
26. Chicheportiche Y, Bourdon PR, Xu H, et al. TWEAK, a new secreted ligand in the tumor necrosis factor family that weakly induces apoptosis. *J Biol Chem*. 1997;272:32401–32410. doi:10.1074/jbc.272.51.32401
27. Ruiz-Andres O, Suarez-Alvarez B, Sánchez-Ramos C, et al. The inflammatory cytokine TWEAK decreases PGC-1α expression and mitochondrial function in acute kidney injury. *Kidney Int*. 2016;89:399–410. doi:10.1038/ki.2015.332
28. Panguluri SK, Bhatnagar S, Kumar A, et al. Genomic profiling of messenger RNAs and microRNAs reveals potential mechanisms of TWEAK-induced skeletal muscle wasting in mice. *PLoS One*. 2010;5:e8760. doi:10.1371/journal.pone.0008760
29. Yadava RS, Foff EP, Yu Q, et al. TWEAK/Fn14, a pathway and novel therapeutic target in myotonic dystrophy. *Hum Mol Genet*. 2015;24:2035–2048.
30. Sato S, Ogura Y, Tajrishi MM, et al. Elevated levels of TWEAK in skeletal muscle promote visceral obesity, insulin resistance, and metabolic dysfunction. *FASEB J*. 2015;29:988–1002. doi:10.1096/fj.14-260703
31. Pascoe AL, Johnston AJ, Murphy RM. Controversies in TWEAK-Fn14 signaling in skeletal muscle atrophy and regeneration. *Cell Mol Life Sci*. 2020;77:3369–3381. doi:10.1007/s00018-020-03495-x
32. Xuekelati S, Maimaitiwusiman Z, Bai X, et al. Sarcopenia is associated with hypomethylation of TWEAK and increased plasma levels of TWEAK and its downstream inflammatory factor TNF-α in older adults: a case-control study. *Exp Gerontol*. 2024;188:112390. doi:10.1016/j.exger.2024.112390
33. Ma L, Maimaitiwusiman Z, Xuekelati S, et al. TWEAK/Fn14 hypomethylation and higher plasma TWEAK and TNF-α levels are related to sarcopenic obesity in community-dwelling elderly in Xinjiang. *Medicine*. 2025;104:e42937. doi:10.1097/MD.0000000000042937
34. Wisniacki N, Amaravadi L, Galluppi GR, et al. Safety, tolerability, pharmacokinetics, and pharmacodynamics of anti-TWEAK monoclonal antibody in patients with rheumatoid arthritis. *Clin Ther*. 2013;35(8):1137–1149. doi:10.1016/j.clinthera.2013.06.008
35. Nguyen MT, Min KH, Lee W. MiR-96-5p induced by palmitic acid suppresses the myogenic differentiation of C2C12 myoblasts by targeting FHL1. *Int J Mol Sci*. 2020;21:9445. doi:10.3390/ijms21249445
36. Davalli P, Mitic T, Caporali A, et al. ROS, cell senescence, and novel molecular mechanisms in aging and age-related diseases. *Oxid Med Cell Longev*. 2016;2016:3565127. doi:10.1155/2016/3565127
37. Chapman J, Fielder E, Passos JF. Mitochondrial dysfunction and cell senescence: deciphering a complex relationship. *FEBS Lett*. 2019;593:1566–1579. doi:10.1002/1873-3468.13498
38. Wan J, Cheng C, Li X, et al. Lactate ameliorates palmitate-induced impairment of differentiative capacity in C2C12 cells through the activation of voltage-gated calcium channels. *J Physiol Biochem*. 2024;80:349–362. doi:10.1007/s13105-024-01009-y
39. Kong S, Cai B, Nie Q. PGC-1α affects skeletal muscle and adipose tissue development by regulating mitochondrial biogenesis. *Mol Genet Genomics*. 2022;297:621–633. doi:10.1007/s00438-022-01878-2
40. Migliavacca E, Tay SKH, Patel HP, et al. Mitochondrial oxidative capacity and $NAD^+$ biosynthesis are reduced in human sarcopenia across ethnicities. *Nat Commun*. 2019;10(1):5808. doi:10.1038/s41467-019-13694-1
41. Tajrishi MM, Zheng TS, Burkly LC, et al. The TWEAK-Fn14 pathway: a potent regulator of skeletal muscle biology in health and disease. *Cytokine Growth Factor Rev*. 2014;25:215–225. doi:10.1016/j.cytogfr.2013.12.004
42. Hu NF, Chang H, Du B, et al. Tetramethylpyrazine ameliorated disuse-induced gastrocnemius muscle atrophy in hindlimb unloading rats through suppression of Ca2+/ROS-mediated apoptosis. *Appl Physiol Nutr Metab*. 2016;42:117–127. doi:10.1139/apnm-2016-0363

43. Dogra C, Hall SL, Wedhas N, et al. Fibroblast growth factor inducible 14 (Fn14) is required for the expression of myogenic regulatory factors and differentiation of myoblasts into myotubes: evidence for TWEAK-independent functions of Fn14 during myogenesis. *J Biol Chem*. 2007;282:15000–15010. doi:10.1074/jbc.M608668200
44. Girgenrath M, Weng S, Kostek CA, et al. TWEAK, via its receptor Fn14, is a novel regulator of mesenchymal progenitor cells and skeletal muscle regeneration. *EMBO J*. 2006;25:5826–5839. doi:10.1038/sj.emboj.7601441
45. Kharel P, Jia C, Dhital KR, et al. TWEAK progress in dermatology: a review. *Indian J Dermatol*. 2023;68:425–429. doi:10.4103/ijd.ijd_885_22
46. Chacón MR, Richart C, Gómez JM, et al. Expression of TWEAK and its receptor Fn14 in human subcutaneous adipose tissue: relationship with other inflammatory cytokines in obesity. *Cytokine*. 2006;33:129–137. doi:10.1016/j.cyto.2005.12.005
47. Bennett G, Strissel KJ, DeFuria J, et al. Deletion of TNF-like weak inducer of apoptosis (TWEAK) protects mice from adipose and systemic impacts of severe obesity. *Obesity*. 2014;22:1485–1494. doi:10.1002/oby.20726
48. Cantó C, Gerhart-Hines Z, Feige JN, et al. AMPK regulates energy expenditure by modulating $NAD^+$ metabolism and SIRT1 activity. *Nature*. 2009;458:1056–1060. doi:10.1038/nature07813
49. Yu B, Jia S, Sun T, et al. Sarcopenic obesity is associated with cardiometabolic multimorbidity in Chinese middle-aged and older adults: a cross-sectional and longitudinal study. *J Nutr Health Aging*. 2024;28:100353. doi:10.1016/j.jnha.2024.100353
50. Weinheimer EM, Sands LP, Campbell WW. A systematic review of the separate and combined effects of energy restriction and exercise on fat-free mass in middle-aged and older adults: implications for sarcopenic obesity. *Nutr Rev*. 2010;68:375–388. doi:10.1111/j.1753-4887.2010.00298.x
51. Zamboni M, Mazzali G, Brunelli A, et al. The role of crosstalk between adipose cells and myocytes in the pathogenesis of sarcopenic obesity in the elderly. *Cells*. 2022;11:3361. doi:10.3390/cells11213361
52. Xuekelati S, Abulitifu Y, Maimaitiwusiman Z, et al. Causal implication of CD52-driven immune dysregulation in sarcopenic obesity: integrating Mendelian randomization and multiomics profiling. *Clin Interv Aging*. 2026;21:570497. doi:10.2147/CIA.S570497
53. Rolland Y, Dray C, Vellas B, et al. Current and investigational medications for the treatment of sarcopenia. *Metabolism*. 2023;149:155597. doi:10.1016/j.metabol.2023.155597
54. Meijboom KE, Sutton ER, McCallion E, et al. Dysregulation of Tweak and Fn14 in skeletal muscle of spinal muscular atrophy mice. *Skelet Muscle*. 2022;12:18. doi:10.1186/s13395-022-00301-z
55. Galluppi GR, Wisniacki N, Stebbins C. Population pharmacokinetic and pharmacodynamic analysis of BIIB023, an anti-TNF-like weak inducer of apoptosis (anti-TWEAK) monoclonal antibody. *Br J Clin Pharmacol*. 2016;82:118–128. doi:10.1111/bcp.12914
56. Kato M, Ishikawa S, Shen Q, et al. In situ-formable, dynamic crosslinked poly (ethylene glycol) carrier for localized adeno-associated virus infection and reduced off-target effects. *Commun Biol*. 2023;6:508. doi:10.1038/s42003-023-04851-w
57. Giacosa A, Barrile GC, Mansueto F, et al. The nutritional support to prevent sarcopenia in the elderly. *Front Nutr*. 2024;11:1379814. doi:10.3389/fnut.2024.1379814
58. Hu J, Wang Y, Ji X, et al. Non-pharmacological strategies for managing sarcopenia in chronic diseases. *Clin Interv Aging*. 2024;19:827–841. doi:10.2147/CIA.S455736